Atmos. Chem. Phys. Discuss., https://doi.org/10.5194/acp-2017-966
Manuscript under review for journal Atmos. Chem. Phys.
Discussion started: 22 December 2017

On the Suitability of Current Atmospheric Reanalyses for Regional Warming Studies over China

Chunlüe Zhou[1], Yanyi He[1], Kaicun Wang[1*]

[1]College of Global Change and Earth System Science, Beijing Normal University, Beijing, 100875, China

***Corresponding Author**: Kaicun Wang, College of Global Change and Earth System Science, Beijing Normal University. Email: kcwang@bnu.edu.cn; Tel.: +86 (10)-58803143; Fax: +86 (10)-58800059.

Atmos. Chem. Phys. Discuss., https://doi.org/10.5194/acp-2017-966
Manuscript under review for journal Atmos. Chem. Phys.
Discussion started: 22 December 2017

Abstract

Reanalyses have been widely used because they add value to the routine observations by generating physically/dynamically consistent and spatiotemporally complete atmospheric fields. Existing studies have extensively discussed their temporal suitability in global change study. This study moves forward on their suitability for regional climate change study where land-atmosphere interactions play a more important role. Here, surface air temperature (T_a) from 12 current reanalysis products were investigated, focusing on spatial patterns of T_a trends, using homogenized T_a from 1979 to 2010 at ~2200 meteorological stations in China. Results show that ~80% of the T_a mean differences between reanalyses and *in-situ* observations are attributed to station and model-grid elevation differences, denoting good skill in T_a climatology and rebutting the previously reported T_a biases. However, the T_a trend biases in reanalyses display spatial divergence (standard deviation=0.15-0.30 ℃/decade at 1°×1° grids). The simulated T_a trend biases correlate well with those of precipitation frequency, surface incident solar radiation (R_s), and atmospheric downward longwave radiation (L_d) among the reanalyses (r=-0.83, 0.80 and 0.77, p<0.1) with their spatial patterns considered. Over southern China, the T_a trend biases (by order of -0.07 ℃/decade) are caused by the trend biases in R_s (by order of 0.10 ℃/decade), L_d (by order of -0.08 ℃/decade) and precipitation frequency (by order of -0.06 ℃/decade). Over northern China, the T_a trend biases (by order of -0.12 ℃/decade) jointly result from those in L_d and precipitation frequency. Therefore, improving simulation of precipitation frequency and R_s helps to maximize regional

Atmos. Chem. Phys. Discuss., https://doi.org/10.5194/acp-2017-966
Manuscript under review for journal Atmos. Chem. Phys.
Discussion started: 22 December 2017

Atmospheric Chemistry and Physics Discussions

climate signal component. Besides, the T_a trend biases show negative spatial correlations (approximately r=-0.26, p=0.00) with inverted trend in NDVI (Normalized Difference Vegetation Index) implying that incorporating vegetation dynamics can advance regional warming modeling. Inclusion of accurate aerosol information in MERRA-2 (Modern-Era Retrospective Analysis for Research and Applications, version 2) helps improve regional climate simulation. ERA-20CM (a twentieth century atmospheric model ensemble without assimilating observations) presents a comparable pattern of the T_a trend biases (standard deviation=0.15 ℃/decade) to ERA-Interim and JRA-55 (the Japanese 55-year Reanalysis) that assimilating some T_a observations, which indicates perturbed physical ensemble technique significantly narrows regional warming uncertainties in reanalyses.

Atmos. Chem. Phys. Discuss., https://doi.org/10.5194/acp-2017-966
Manuscript under review for journal Atmos. Chem. Phys.
Discussion started: 22 December 2017

1. Introduction

Observations and models are two fundamental approaches to understand climate change. The observations directly link with climate system via measuring instruments and models has an indirect link by involving information received from measurement, prior knowledge and theory.

A large number of meteorological observations have been accumulated, including near-surface and upper-air temperature, humidity, wind and pressure from a variety of sources-surface stations, ships, buoys, radiosondes and airplanes. They constitute a major source of atmospheric information through the depth of troposphere but suffer from incomplete spatiotemporal coverage and observed errors including systematic, random and representative errors. Recent satellite-based observations have much better coverage but suffer from other limitations including notably temporal inhomogeneity (e.g., satellite drift) and retrieval error (Bengtsson et al., 2007). These space-time-varying gaps restrict the observation alone to be effectively applied in climate research.

To fill in the gaps in the observations, a model is needed. The model can be very simple, e.g., linear interpolation or geo-statistical approaches based on the spatial and temporal autocorrelation of the observations. However, these models lack necessary dynamical/physical mechanisms. With steady progress in the numerical weather prediction (NWP) model in charactering the global atmospheric circulation in the early 1980s (Bauer et al., 2015), an original generation of ‘reanalysis’ was achieved by combining observations and dynamic models to provide the first global

Atmos. Chem. Phys. Discuss., https://doi.org/10.5194/acp-2017-966
Manuscript under review for journal Atmos. Chem. Phys.
Discussion started: 22 December 2017

atmospheric datasets available for scientific research (Bengtsson et al., 1982a, b).

After realizing the great value of this kind of reanalysis for atmospheric research, a step forward was taken with the suggestion made by Bengtsson and Shukla (1988) and Trenberth and Olson (1988) that most meteorological observations should be optimally assimilated under a fixed dynamical system over a period of time long enough to be useful for climate studies. In this way available observations are ingested by advanced data-assimilation techniques to provide a continuous initial state for the NWP model to produce the next short-term forecast, thus generating physically consistent and spatiotemporally complete three-dimensional atmospheric fields that are updated in light of observations.

Under this guide, successive generations of atmospheric reanalyses established by several institutes have improvements in quality with better observation integrity, better models and better assimilation methods since the mid-1990s. These include the first two generations of global reanalyses from the National Centers for Environmental Prediction [NCEP-R1 (Kalnay et al., 1996) and NCEP-R2 (Kanamitsu et al., 2002)], the European Centre for Medium-Range Weather Forecasts (ECMWF) [ERA-15 (Gibson et al., 1997), ERA-40 (Uppala et al., 2005) and ERA-Interim (Dee et al., 2011b)], the Japanese Meteorological Agency [JRA-25 (Onogi et al., 2007) and JRA-55 (Kobayashi et al., 2015)] and the National Aeronautics and Space Administration [MERRA (Rienecker et al., 2011)].

These reanalyses produce multiple time-scaled, global gridded datasets including a large variety of atmosphere, sea and land surface parameters, many of which are not easily or routinely observed but dynamically constrained by a great number of multiple sourced observations assimilated under a fixed NWP model. During the data assimilation, prior information about uncertainties in observations and model are used for quality checks, to derive bias adjustments and to assign their proportional weights. Therefore, such reanalyses add value to the instrumental record in the aspects of bias adjustment, spatiotemporal coverage and dynamical integrality/consistency.

Previous studies have revealed that such reanalyses have contributed significantly to a more detailed and comprehensive understanding of the dynamics of the Earth's atmosphere (Dee et al., 2011b;Kalnay et al., 1996;Nguyen et al., 2013;Kidston et al., 2010;Simmonds and Keay, 2000;Simmons et al., 2010;Mitas and Clement, 2006). Extensive assessment studies reported that most reanalyses have a certain level of performance in absolute value (Betts et al., 1996;Zhou and Wang, 2016a;Betts et al., 1998), interannual variability (Lin et al., 2014;Lindsay et al., 2014;Zhou and Wang, 2017a, 2016b;Wang and Zeng, 2012), distribution (Gervais et al., 2014;Heng et al., 2014;Mao et al., 2010) and relationship of inter-variables (Niznik and Lintner, 2013;Cash et al., 2015;Zhou et al., 2017a;Zhou and Wang, 2016a;Betts, 2004) over regions worldwide. However, there are still certain errors in these aspects so as to restrict their general use, especially for climate applications.

These errors emerging in reanalysis products can be summarized into three sources: observation error, model error and assimilation error (Thorne and Vose, 2010;Parker, 2016;Lahoz and Schneider, 2014;Dee et al., 2014;Zhou et al., 2017a). Specially, the observation error incorporates systematic/random error in instrument

Atmos. Chem. Phys. Discuss., https://doi.org/10.5194/acp-2017-966
Manuscript under review for journal Atmos. Chem. Phys.
Discussion started: 22 December 2017

and its replacement, error in data reprocessing and representative error in spatiotemporal incompleteness (Dee and Uppala, 2009;Desroziers et al., 2005); the model error mainly refers to inadequate representation of physical processes in the NWP model (Peña and Toth, 2014;Bengtsson et al., 2007), e.g., lack of time-varying setting of surface conditions [such as vegetation growth (Zhou and Wang, 2016a;Trigo et al., 2015)] and incomplete cloud-precipitation-radiation parameterization (Fujiwara et al., 2017;Dolinar et al., 2016); the assimilation error involves mapping error of model space to observation space and error in the topology of the cost function (Dee, 2005;Dee and Da Silva, 1998;Lahoz and Schneider, 2014;Parker, 2016).

These reanalyses above consist of the true climate signal and some nonlinear interactions among observation error, model error, and assimilation error during the assimilation process. These time-varying errors can thus introduce a fictitious trend without being eliminated by the data assimilation system. Many spurious variations in the climate signal have been also identified in the early-generation reanalyses (Bengtsson et al., 2004;Andersson et al., 2005;Chen et al., 2008;Zhou and Wang, 2016b, 2017a;Zhou et al., 2017a;Schoeberl et al., 2012;Xu and Powell, 2011;Hines et al., 2000;Cornes and Jones, 2013). Therefore, the reanalysis under the guide of the existing reanalysis strategy may not accurately capture the climate trends (Trenberth et al., 2008), even though having a relatively accurate estimate of synoptic or interannual variations of the Earth's atmosphere.

An emerging requirement for climate applications of reanalysis data is the

Atmos. Chem. Phys. Discuss., https://doi.org/10.5194/acp-2017-966
Manuscript under review for journal Atmos. Chem. Phys.
Discussion started: 22 December 2017

accurate representation of decadal variability, further increasing the confidence in the estimate of climate trends. This kind of climate-quality reanalysis is required to be to great extent free of other spurious non-climatic signals introduced by changing observations, imperfect model and assimilation error, i.e., to keep the time consistency. Therefore, the extent to which the estimate of climate trends by the climate-quality reanalysis can be realized attracts much attention and sparks heated debates (Thorne and Vose, 2010;Dee et al., 2011a;Dee et al., 2014;Bengtsson et al., 2007).

With great progress in climate forecast model (more accurate representation of climate change and variability) and coupled data assimilation, a lot of efforts has been made by several institutes to build the consistent climate quality reanalysis under the climate strategy that assimilating few but high-quality long-term observations. New generation of climate quality reanalyses extend back to the late nineteenth century and are from the National Centers for Environmental Prediction [CFSR (Saha et al., 2010)], the University of Colorado's Cooperative Institute for Research in Environmental Sciences (CIRES) together with the National Oceanic and Atmospheric Agency (NOAA) [NOAA 20CRv2c (Compo et al., 2011)] and the ECMWF [ERA-20C (Poli et al., 2016), ERA-20CM (Hersbach et al., 2015) and CERA-20C (Laloyaux et al., 2016)]. Compo et al. (2013) suggested that the NOAA 20CRv2c can reproduce the trend in global mean surface air temperature. In addition, the uncertainties estimated from multiple ensembles are provided to increase the confidence of the climate trends (Thorne and Vose, 2010;Dee et al., 2014).

From the conventional NWP reanalysis to the climate quality reanalysis, existing researches mainly focus on comparing the differences in temporal variability between reanalyses and observations, using some statistical metrics, e.g., mean values, standard deviations, interannual correlations, probability density functions and trends of surface air temperature over regions worldwide. These evaluations actually provide an insight into the temporal evolution of the Earth's atmosphere. However, it lacks the performance evaluation of reanalysis in representing spatial patterns of these statistics associated with the role of land-atmosphere and dynamical processes of climate system. Moreover, the assessment of these spatial patterns provides a direct way to examine the most distinguished advantage of reanalysis that the geo-statistical interpolation does not have, and thereby the assessment of the spatial patterns remains to be comprehensively investigated.

Using the highly-dense station-based datasets including surface air temperature (T_a), surface incident solar radiation (R_s), surface downward longwave radiation (L_d), precipitation from 1979 to 2010 at ~2200 meteorological stations over China, this study provides a quantitative examination of the simulated patterns of T_a variations from the conventional NWP to climate quality reanalyses, including climatology, interannual variability, mutual relationship between relevant quantities, long-term trends and their controlling factors. The results identified strength and weakness of the current reanalyses in regional climate change studies and provide possible ways to improve reanalyses in the near future.

2. Data and Methods

Atmos. Chem. Phys. Discuss., https://doi.org/10.5194/acp-2017-966
Manuscript under review for journal Atmos. Chem. Phys.
Discussion started: 22 December 2017

2.1 Observation Datasets

The latest comprehensive daily dataset (average at 0, 6, 12, 18 UTC) including T_a, precipitation, sunshine duration, relative humidity, water vapor pressure, surface pressure and cloud fraction from approximately 2400 meteorological stations in China from 1961 to 2014, was obtained from the China Meteorological Administration (CMA, http://data.cma.cn/data). Approximately 2200 stations with complete and homogeneous data were selected in this study (Wang and Feng, 2013;Wang, 2008;Wang et al., 2007). High density of meteorological stations in China is beneficial to represent and assess the simulated skill of regional patterns in surface warming by reanalysis.

The R_s based on the revised Ångström-Prescott equation (Wang et al., 2015;Yang et al., 2006;Wang, 2014) was used in this study. The derived R_s has considered the effects of Rayleigh scattering, water vapor absorption and ozone absorption (Wang et al., 2015;Yang et al., 2006) and can accurately reflect the impact of aerosols and clouds on R_s over China (Wang et al., 2012;Tang et al., 2011). Several intensive studies have reported that the derived R_s can accurately depict the interannual, decadal and long-term variances of R_s (Wang et al., 2015;Wang, 2014;Wang et al., 2012).

The L_d is typically estimated by first determining the clear-sky radiation and atmospheric emissivity (Brunt, 1932;Choi et al., 2008;Bilbao and De Miguel, 2007), and then correcting for cloud fraction (Wang and Liang, 2009;Wang and Dickinson, 2013). The derived L_d can directly reflect greenhouse effect of atmosphere water vapor and clouds. Additionally, a precipitation event was defined as one day with precipitation of at least 0.1 mm daily in this study, which was shown as a good indicator in reflecting precipitation impact on interannual variability and trend of T_a (Zhou et al., 2017a). In all, the derived R_s and L_d are able to physically quantify solar radiative effect and greenhouse effect on surface warming. Precipitation frequency can regulate the partitioning of available energy into latent and sensible heat fluxes, and then modulate the variance of T_a (Zhou et al., 2017a;Zhou and Wang, 2017a).

2.2 Reanalysis Products

All the major global atmospheric reanalysis products were included in this study (Table 1). The reanalyses were summarized below from three aspects, i.e., observation assimilated, forecast model and assimilated method. The conventional NWP reanalyses assimilated many of multi-sourced conventional and satellite data (Table 1), whose spatiotemporal errors vary with time, to characterize the basic upper-air atmospheric fields. In particular, the ERA-Interim and JRA-55 incorporate some observations of T_a and the MERRA2 assimilates aerosol optical depth from satellite retrievals and model simulation based on emission inventory, whereas most others use the climatological aerosol (Table 1). To derive long-term consistent climate signal, the new strategy that the climate quality reanalyses adopt is to assimilate few but homogeneous observations, e.g., surface pressure (Table 1). Except for no assimilation of surface pressure, ERA-20CM has the same forecast model and external forcings as ERA-20C (Table 1), so inclusion of ERA-20CM here will provide an insight into the suitability of current atmospheric reanalyses in regional warming studies.The reanalyses adopt different sea surface temperatures (SSTs) and sea ice concentrations for different time periods, maybe leading to temporal discontinuities in climate signal derived from the reanalyses (Table 1). To address this issue, the boundary condition in the CFSR is generated by its coupled ocean-sea ice models instead of the observation (Table 1). The CFSR, NOAA 20CRv2c and NOAA 20CRv2 use the monthly greenhouse gases (GHGs) with annual mean near the CMIP5; the ERA-Interim has a slower increase of GHGs than the CMIP5 after 2000; the NCEP-R1 and NCEP-R2 adopt constant global mean of GHGs (Table 1).

The forecast model is a fundamental component of reanalysis that provides the background fields to the assimilation system. The reanalyses in an institute generally use similar but updated physical parameterizations and higher spatial resolution in newer generations (Table 1). The assimilation methods adopted by the current reanalyses incorporate variational methods (3D-Var and 4D-Var) and the Ensemble Kalman Filter (EnKF) (Table 1).

The 2-m T_a in NCEP-1, NCEP-2, MERRA, MERRA-2, ERA-20C, ERA-20CM, CERA-20C, NOAA 20CRv2c, NOAA 20CRv2 and CFSR are model-derived fields as a function of surface skin temperature and the temperature at the lowest model level, vertical stability and surface roughness that were primarily constrained by observations of upper air variables and surface pressure (Kanamitsu et al., 2002;Rienecker et al., 2011;Reichle et al., 2017;Poli et al., 2016;Hersbach et al., 2015;Laloyaux et al., 2016;Compo et al., 2011;Saha et al., 2010). Yet, the T_a in ERA-Interim and JRA-55 are post-processing products by linear interpolation between the lowest model level and the surface, assimilated with some ground-based observations of T_a, with the help of Monin-Obukhov similarity profiles consistent with the model's parameterization of the surface layer (Dee et al., 2011b;Kobayashi et al., 2015). Additionally, radiation calculations are diagnostically determined from the prognostic cloud condensate microphysics parameterization and cloud macrophysics assumes a maximum-random cloud overlapping scene (Saha et al., 2010;Dolinar et al., 2016).

2.3 Method to Homogenize the Observed Time Series

The problems related to the observation infrastructure (e.g., instrument aging and changes in observing practices) and station relocations can also lead to false time-heterogeneity in time series. Therefore, it's necessary to diminish the impact of data homogenization on the trends in the observed variables during the study period 1979-2010.

We used the RHtestsV4 software package (Wang and Feng, 2013) to detect and homogenize the breakpoints in the monthly time series. The package involves two algorithms: the PMFred algorithm is based on the penalized maximal *F*-test (*PMF*) without a reference series (Wang, 2008) and the PMTred algorithm is based on the penalized maximal *t*-test (*PMT*) with a reference series (Wang et al., 2007).

In this study, we first used the PMFred to find potential reference series at the 95% significant level. Then, we reconstructed homogenous series for each inhomogeneous series by the following steps: 1) less than 110km horizontally distant from the inhomogeneous station and 500m vertical height difference; 2) correlation coefficient over 0.9 of the first-order difference in homogeneous series with that in the inhomogeneous one; 3) the first ten homogeneous series was inverse-distance-weightedly averaged as reference series for the inhomogeneous one. Finally, we applied the PMTred algorithm to test all the inhomogeneous series with the reference series nearby. Several intensive researches were conducted to show a good performance of the PMTred algorithm in detecting change points of inhomogeneous series (Venema et al., 2012;Wang et al., 2007).

If the breakpoint is statistically significant, the quantile-matching (QM) adjustment in RHtestsV4 is recommended for making adjustments to the time series (Wang et al., 2010;Wang and Feng, 2013), based on the longest available segment from 1979 to 2010 as the base segment. The QM adjustment aims to match the empirical distributions from all detrended segments with the specific base segment (Wang et al., 2010). In addition, we replicated the procedures above for the sparse stations over western China and Tibetan Plateau. Recently, the PMTred algorithm with the QM adjustment was successfully used to homogenize climatic time series (Aarnes et al., 2015;Tsidu, 2012;Dai et al., 2011;Siswanto et al., 2015;Wang and Wang, 2016;Zhou et al., 2017a).

As such, the significant breakpoints over 1092 out of 2193 (49.8%) stations were detected and adjusted at a confidence level of 95% for the T_a time series, 1079 out of 2193 (49.2%) stations for R_s, 64 out of 2193 (2.9%) stations for precipitation frequency, 971 out of 2193 (44.2%) stations for L_d, 944 out of 2193 (43.0%) stations for water vapor pressure, 956 out of 2193 (43.6%) stations for cloud fraction.

2.4 Trend Calculation, Partial Linear Regression, Total Least Squares

Atmos. Chem. Phys. Discuss., https://doi.org/10.5194/acp-2017-966
Manuscript under review for journal Atmos. Chem. Phys.
Discussion started: 22 December 2017

Atmospheric Chemistry and Physics
Discussions

The bias, root-mean-square error (*RMSE*), standard deviation and correlation coefficient (*r*) were used to assess the absolute value of T_a. Trends in T_a and relevant variables were calculated using the ordinary least squares method (OLS) and the two-tailed Student's *t*-test.

The partial least squares approach was used to investigate the net relationship of detrended T_a with relevant variables (R_s, L_d and precipitation frequency) after statistically excluding the confounding effects among relevant variables (Zhou et al., 2017a). To evaluate potential colinearity of independent variables in the regress model, the variance inflation factor (*VIF*) was calculated. The *VIFs* for R_s, precipitation frequency and L_d were less than 4, e.g., *VIFs* of 2.19 for China, much less than the threshold of 10, above which the collinearity of the regress models is bound to adversely affect the regression results (Ryan, 2008).

The Pearson correlation analysis was used to reveal the spatial relationship of T_a with relevant variables. To further investigate the relationship of spatial distributions of the T_a trend biases with the relevant parameters among the twelve reanalysis products, the weighted total least square (WTLS) were adopted, in which the spatial uncertainties and correlations in both variables were included (Reed, 1989;York et al., 2004;Golub and Van Loan, 1980;Hyk and Stojek, 2013;Tellinghuisen, 2010):

$$\omega(x_i) = 1/\hat{\sigma}_{x_i}^2 \tag{1}$$

$$\omega(y_i) = 1/\hat{\sigma}_{y_i}^2 \tag{2}$$

$$W_i = \frac{\omega(x_i)\cdot\omega(y_i)}{\omega(x_i) + b^2\omega(y_i) - 2b\cdot r_i\sqrt{\omega(x_i)\cdot\omega(y_i)}} \tag{3}$$

$$U_i = x_i - \sum_i^n (W_i \cdot x_i) \Big/ \sum_i^n (W_i) \tag{4}$$

$$V_i = y_i - \sum_i^n (W_i \cdot y_i) \Big/ \sum_i^n (W_i) \tag{5}$$

$$\beta_i = W_i [\frac{U_i}{\omega(y_i)} + \frac{b \cdot V_i}{\omega(x_i)} - (b \cdot U_i + V_i) \frac{r_i}{\sqrt{\omega(x_i) \cdot \omega(y_i)}}] \tag{6}$$

$$b = \frac{\sum_{i=1}^n W_i \cdot \beta_i \cdot V_i}{\sum_{i=1}^n W_i \cdot \beta_i \cdot U_i} \tag{7}$$

where x_i and y_i are median trends in x and y variable (including T_a, R_s and so on) at i^{th} reanalysis product, $\hat{\sigma}_{x_i}$, $\hat{\sigma}_{x_i}$ and r_i are spatial standard deviations and correlations of trends in x and y variables at i^{th} reanalysis product, β_i is the least-squares-adjusted value and W_i is the weight of the residual error, b is the slope estimated by iterative method with relative tolerance of 10^{-16}.

The Monte Carlo method with 10000 experiments was applied to estimate the 90% confidence intervals of the slope b. In the Monte Carlo method, the grid index is generated as random number, i.e., the 1-691 grid index over China, based on which we could sample the spatial pattern in trends biases in T_a, R_s, L_d and precipitation frequency. Then, we calculated the median trends and their spatial standard deviations and correlations for each experiment, used in the WTLS.

3. Results

3.1 Elevation Difference Dependency of Surface Air Temperature Bias

Fig. 1 illustrates differences in T_a from the conventional NWP reanalysis and climate quality reanalysis relative to the homogenized station-based observations over China during the period 1979-2010. If directly compare the T_a at model grids and stations, the reanalysis products exhibit an underestimated T_a over most regions of China (-0.28 ℃ to -2.56 ℃ in China), especially over Tibetan Plateau (-2.75 ℃ to -7.00 ℃) and Middle China (-1.19 ℃ to -2.91 ℃) (Fig. 1 and Table 2). A homogeneous adjustment of 0.03 ℃ from the raw T_a observations is insufficient to cancel the underestimation of T_a by the reanalyses (Fig. 1 and Table 2). The similar results of T_a bias have been widely reported by previous studies over regions worldwide (Mao et al., 2010;Pitman and Perkins, 2009;Reuten et al., 2011;Wang and Zeng, 2012;Zhou et al., 2017a;Zhou and Wang, 2016a).

However, we found that the spatial patterns in the differences in T_a are well correlated with the elevation differences between models and stations with correlation coefficients (r) of 0.85 to 0.94 (Figs. 2 and S1), which is in accordance with the reports from NCEP-R1, NCEP-R2 and ERA-40 (You et al., 2010;Ma et al., 2008;Zhao et al., 2008). The elevation difference (ΔHeight, Figs. 2 and S1) between station and model grid consists of the filtering error in spectral model elevation (Δf) and difference in site-to-grid elevation (Δs) due to complex orography. We further quantified their relative contribution to the T_a differences. The elevation difference can explain approximately 80% of the T_a difference, among which approximately 74% is from the site-to-grid elevation difference and approximately 6% is from the filtering error in spectral model elevation (Fig. 2).

One can find that the regressed coefficient of the differences in T_a is approximately 6 ℃/1km, near to the lapse rate at surface (Fig. 2). The lapse rate over 6 ℃/1km can be seen over Tibetan Plateau (Fig. 2, in red dots). This result is very consistent with the reported lapse rate over China (Li et al., 2015;Fang and Yoda, 1988). In addition, the decreasing rate in model filtering error is approximately 4 ℃/1km among the twelve reanalysis (Fig. 2). These results above have an important implication for a good skill in the simulation of climatology of T_a in the twelve reanalyses over China.

3.2 Comparison of Regional-scale Surface Air Temperature Series

Fig. 3 shows the Taylor diagrams of annual T_a anomalies from the observations and reanalyses over China and its seven subregions. We found that the correlations of annual T_a anomalies between the twelve reanalysis products and the observations are prettily strong with median r of 0.95 (Fig. 3), despite of relatively weak correlation over Tibetan Plateau for NCEP-R2 (r=0.24) and CFSR (r=0.53). The simulated time series of T_a anomalies over eastern China are depicted most accurately by the reanalyses (Fig. 3c-g).

Overall, the conventional NWP reanalyses (denoted by number 3-7) have a better skill than the climate quality reanalysis (denoted by number 8-14) at this aspect (Fig. 3). The ERA-Interim and JRA-55 has the best performance in the simulated time series of T_a anomalies over China (r=1.00, RMSE=0.05 ℃) and seven regions (r=0.98, RMSE=0.1 ℃) (Fig. 3), mainly due to the post-processing of assimilated surface air temperature in ERA-Interim and JRA-55 (Table 1).

Compared with the T_a from MERRA2 to MERRA, we found that the MERRA2

Atmos. Chem. Phys. Discuss., https://doi.org/10.5194/acp-2017-966
Manuscript under review for journal Atmos. Chem. Phys.
Discussion started: 22 December 2017

has an improved performance over Northern China by an increasing correlation coefficient of 0.1 and a reduced RMSE of 0.1 ℃ (Fig. 3), maybe because the MERRA2 assimilated the time-varying aerosol loading (Balsamo et al., 2015;Reichle et al., 2011). However, this circumstance does not improve over Southeast China (Fig. 3h).

The CERA-20C has a better performance than ERA-20C and ERA-20CM, may due to an inclusion of coupled climate forecast model and data assimilation, as well as surface pressure assimilated in CERA-20C (Fig. 3 and Table 1). The NOAA 20CRv2c and NOAA 20CRv2 have a moderate performance in this aspect (r=0.8, RMSE=0.3 ℃) (Fig. 3) and the former has no improved performance despite of the use of new boundary condition (Compo et al., 2011).

3.3 Key Factors Regulating Regional Temperature Change

This section discusses key factors controlling regional temperature change from a perspective of energy balance and its partitioning. The R_s heats the surface and the surface heats the air near surface by partitioning into sensible heat flux (Zhou and Wang, 2016a;Wang and Dickinson, 2013;Zhou and Wang, 2016c). The part of energy absorbed by the surface is released back to Space as outgoing longwave radiation, some of which is reflected by clouds and is influenced by atmospheric water vapor, further warming near-surface air (Wang and Dickinson, 2013), known as greenhouse effect (quantified by the L_d) on T_a. Existing studies have suggested that precipitation frequency is a better factor in quantifying interannual variability of soil moisture over China than precipitation amount (Wu et al., 2012;Piao et al., 2009;Zhou et al.,

Atmos. Chem. Phys. Discuss., https://doi.org/10.5194/acp-2017-966
Manuscript under review for journal Atmos. Chem. Phys.
Discussion started: 22 December 2017

2017a;Zhou and Wang, 2017a), and then changes vegetation growth and surface characteristics (e.g. surface albedo and roughness). These changes would alter the partitioning of available energy for regulating the change in T_a.

Figs. 4 illustrates the partial relationships between the annual T_a and R_s anomalies, the precipitation frequency and L_d. Results show that the T_a has consistently positive correlations with the R_s (except over the Tibetan Plateau) and L_d, but has consistently negative correlations with precipitation frequency in observations and the twelve reanalysis products (Fig. 4). Based on the observations, the interannual variance of T_a is jointly determined by precipitation frequency and L_d in Northeast China and northern part of Northwest China (Fig. 4). All of the reanalyses roughly capture these factors over these regions, even though having differences in relative magnitudes (Fig. 4), i.e., ERA-20CM, NOAA 20CRv2c, NOAA 20CRv2 and CFSR exhibit comparably relationships of T_a with precipitation frequency and L_d, but MERRA, MERRA2, NCEP-R2, ERA-20C, and CERA-20C exhibit overestimated relationships of T_a with precipitation frequency and ERA-Interim, JRA-55, and NCEP-R1 present overestimated relationships of T_a with L_d over these regions (Fig. 4).

Over North China Plain and Middle China, the interannual variance of T_a is jointly determined by R_s, the precipitation frequency and L_d (Fig. 4). The reanalyses roughly capture these three factors on T_a, despite of diverse combinations (Fig. 4). Among these combination, the JRA-55, MERRA2, ERA-20CM and ERA-Interim is comparable to the observations over these regions (Fig. 4). Over Southeast China, the interannual variance of T_a is primarily regulated by L_d, the precipitation frequency and

R_s (Fig. 4). The reanalyses exhibit slightly overestimated relationships of T_a with R_s and underestimated relationships with the precipitation frequency (Fig. 4).

Over Tibetan Plateau, the interannual variance of T_a is regulated by R_s and the precipitation frequency (Fig. 4). Most reanalyses roughly capture the combinations of these factors, but exhibit a certain difference in relative impact of R_s and the precipitation frequency on T_a (Fig. 4). MERRA, MERRA2, NOAA 20CRv2c and NOAA 20CRv2 overestimate the relationships of T_a with R_s over Tibetan Plateau (Fig. 4).

Overall, the spatial patterns of the simulated partial correlation of T_a with R_s in reanalysis products significantly correlated with those from the observations (r=0.13-0.35, p<0.05 for the conventional NWP reanalysis and larger r=0.24-0.41, p<0.05 for the climate quality reanalysis), and the spatial patterns in the sensitivity of T_a to R_s exhibit the significant correlations for most climate quality reanalysis (r=0.12-0.17, p<0.05) (Table 1). The largest spatial correlations of the sensitivity of T_a to these three relevant parameters in the reanalyses is found to the precipitation frequency (r=0.16-0.43, p<0.05) (Table 3). The significant spatial correlations of the relationships (including partial correlation and sensitivity) of T_a with L_d were also found (Table 1).

3.4 Regional Warming Trend Biases and Their Causes

The T_a exhibits strong warming trends of 0.37 ℃/decade (p<0.05) from the observations and 0.22-0.48 ℃/decade (p<0.05) among the twelve reanalyses from 1979 to 2010 over China (Figs. 5 and S2-S3, Table 2). The ERA-Interim and JRA-55 have spatial correlations with observations (r=0.47 and 0.54, p<0.05) due to the assimilation of T_a, whereas NCEP-R2 and ERA-20C perform worst (Figs. S3, Tables 1 and 3). Furthermore, approximately 87% of the observed T_a trend over China can be explained by the greenhouse effect (i.e., trend in L_d, 65%), the precipitation frequency (29%) and R_s (-7%, due to trend of -1.1 W·m^{-2}/decade) (Figs. S3-4). The greenhouse effect of the observed T_a trend mainly consist of trends in the atmospheric water vapor (42%) and cloud fraction (3%) (Fig. S5). Among the reanalyses, over 90% of the T_a trends can be explained by greenhouse effect, the precipitation frequency and R_s (Figs. S4-6). Specifically, ERA-Interim, JRA-55, MERRA and MERRA2 present the best ability of capturing these contribution to the T_a trend over China, from greenhouse effect (48% to 76%), the precipitation frequency (22% to 34%) and R_s (-4% to 13%) (Figs. S4 and S6). The remaining conventional NWP reanalyses (i.e., NCEP-R1 and NCEP-R2) largely overestimated contribution of the R_s to the T_a trend, whereas the climate quality reanalyses overestimated that from the L_d (Figs. S4 and S6).

However, the averaged trends across a large territory may mask regionally different values, reflecting diverse regional warming biases and the causes (Figs. 5-7). Evidently, mean-adjusted spatial patterns of trend biases in T_a show consistency among the twelve reanalyses (Fig. S7) and mimic spatial patterns in the overestimated R_s trends over the North China Plain, South China and Northeast China (Fig. S8), with their spatial correlation in most reanalyses (r=0.11-0.42, p<0.05) (Figs. 6 and S7-8, Table 3). Howbeit, reanalyses still underestimate the T_a trend over most regions, one of important reasons for which is the increase in precipitation frequency over

Northwest China, the Loess Plateau, Middle China for the conventional NWP reanalyses and over boarder regions for the climate quality reanalyses (Figs. 5-6 and S9). This is reflected by their negative spatial correlation with a maximum of -0.62 (p<0.05, for MERRA) (Table 3). Moreover, the decrease in L_d, due to the decreases in the atmospheric water vapor and cloud fraction in the conventional NWP reanalyses (Figs. S10-12), substantially cancels the warming effect of the overestimated R_s on T_a over eastern China (Figs. 5 and S7). The opposite changes occur over Southeastern China in the climate quality reanalyses (Figs. 5 and S10). This effect of changes in L_d is reflected by their spatial correlations of up to 0.50 (p<0.05) (Table 3).

Here, we further quantified contribution of trend biases in T_a by those in R_s, L_d and the precipitation frequency among the twelve reanalyses over China and its seven subregions (Figs. 6-7). Over China, overestimated R_s trends (by 0.00-3.93 W·m^{-2}/decade, Figs. S8 and S13) can increase the T_a trends (by 0.02-0.16 ℃/decade, Fig. 7) in twelve reanalyses, underestimated L_d trends (by -0.25 to -1.61 W·m^{-2}/decade for the conventional NWP reanalyses, Figs. S10 and S15) can decrease the T_a trends (by -0.05 to -0.25 ℃/decade for the conventional NWP reanalyses, Fig. 7) and precipitation frequency trends biases (by approximately -1.5days/decade for the conventional NWP reanalyses and approximately 2.6 days/decade for the climate quality reanalyses, Figs. S9 and S14) can decrease the T_a trends (by 0.01 to 0.05 ℃/decade for the conventional NWP reanalyses and -0.01 to -0.06 ℃/decade for the climate quality reanalyses, Fig. 7), which jointly make the T_a trends underestimated by the order of 0.10 ℃/decade in reanalyses (Fig. 7 and Table 2).

Atmos. Chem. Phys. Discuss., https://doi.org/10.5194/acp-2017-966
Manuscript under review for journal Atmos. Chem. Phys.
Discussion started: 22 December 2017

Over northern China, trend biases in T_a primarily result from those in precipitation frequency and L_d (Figs. 6-7). Over Northeast China, observations exhibit an amplified warming of 0.41 ℃/decade (p<0.05, Fig. 4 and Table 2), which is significantly underestimated by NCEP-R1, JRA-55, NOAA 20CRv2 and NOAA 20CRv2c (by the order of -0.15 ℃/decade) and is overestimated by MERRA and CFSR (by the order of 0.2 ℃/decade) (Figs. 6-7). These T_a trend biases in reanalysis are jointly explained with the warming (0.04-0.48 ℃/decade) induced by underestimated trends in precipitation frequency and the cooling (-0.04 to -0.42 ℃/decade) by underestimated trends in L_d (Fig. 7).

Over Northwest China, trend biases in precipitation frequency and L_d mainly explained overestimated warming in NCEP-R2 (by 0.22 ℃/decade) (Fig. 7). Largely underestimated trend in L_d induced by the decrease in the atmospheric water vapor and cloud fraction (Figs. S9-S12 and S16-17), leads to an underestimated warming in MERRA (by -0.22 ℃/decade) (Fig. 7).

Most reanalyses present a weakening warming over Tibetan Plateau and Loess Plateau (Fig. 5 and S3, Table 2). More evidently, NCEP-R1 and NCEP-R2 fail to reproduce the warming over Tibetan Plateau and MERRA fails over Loess Plateau (Fig. 5 and S3, Table 2). The significant cooling trend biases in T_a (by -0.02 to -0.31 ℃/decade) over the Tibetan Plateau and Loess Plateau result from underestimated trends in L_d and overestimated trends in precipitation frequency in most reanalyses (Figs. 5-7 and S9-12). This cooling biases are further induced by the underestimated trends in R_s (Figs. 5-7 and S8).

Over southern China, trend biases in T_a are regulated by the trend biases those in R_s, L_d and the precipitation frequency (Figs. 6-7). Over Southeast China, significant overestimated trends in T_a (by 0.04, 0.02 and 0.17 ℃/decade, respectively) are induced by overestimated trend in R_s (by 4.25, 3.34 and 6.27 W·m^{-2}/decade, respectively) in ERA-Interim, JRA-55 and CFSR (Figs. 6-7 and S8). The underestimated trends in T_a are induced by overestimated trends in precipitation frequency and L_d in NCEP-R1, MERRA, ERA-20CM, CERA-20C, NOAA 20CRv2 and NOAA 20CRv2c (Figs. 6-7 and S9).

Over Middle China, significant overestimated trends in T_a (by 0.04, 0.06, 0.11, 0.03, 0.11 and 0.14 ℃/decade, respectively) are induced by overestimated trend in R_s (by 2.09, 1.50, 2.59, 1.20 and 4.81 W·m^{-2}/decade, respectively) in ERA-Interim, JRA-55, ERA-20C, ERA-20CM, CERA-20C and CFSR (Figs. 6-7 and S8). The overestimated trends in precipitation frequency could cool the trends in T_a in reanalyses, especially for MERRA (-0.15 ℃/decade of the induced trend bias) over Middle China (Figs. 6-7 and S9).

Due to underestimated trend in the atmospheric water vapor and cloud fraction (Figs. S11-12), the L_d is underestimated to have a cooling effect on the T_a trend (by -0.05 to -0.32 ℃/decade) in reanalyses over North China Plain (Figs. 6-7 and S10). However, due to the lack of inclusion of the plausible trends in aerosol loading, the substantial increases in R_s over North China Plain (Fig. S8) have a strong warming effect on the T_a trend (by 0.01 to 0.21 ℃/decade) in reanalyses (Figs. 6-7 and S8). The trend biases in precipitation frequency (by approximately -2.5days/decade for the conventional NWP reanalyses and approximately 1.5days/decade for some climate quality reanalyses) contribute some part of trend biases in T_a (by approximately 0.05 ℃/decade for the conventional NWP reanalyses and -0.03 ℃/decade for the climate quality reanalyses).

Overall, trend biases in T_a in reanalyses can be substantially explained by those in L_d, precipitation frequency and R_s, but it varies by regions (Figs. 6-7). Over northern China, trend biases in T_a (by order of -0.12 ℃/decade) primarily result from a combination of those in L_d (by order of -0.10 ℃/decade) and precipitation frequency (by order of 0.05 ℃/decade), with relatively small contribution from R_s (by order of -0.03 ℃/decade). Over southern China, trend biases in T_a (by order of -0.07 ℃/decade) are caused by those in R_s (by order of 0.10 ℃/decade), L_d (by order of -0.08 ℃/decade) and precipitation frequency (by order of -0.06 ℃/decade) (Fig. S18).

3.5 Spatial Linkage of Warming Trend Biases among the Twelve Reanalyses

By integrating relationship of spatial patterns in the T_a trend biases with those in R_s, L_d and precipitation frequency over China among the twelve reanalyses (Fig. 8), it was found that trend biases in T_a show significant correlations with R_s (r=0.80, slope=0.06, p=0.09), precipitation frequency (r=-0.83, slope=-0.04, p=0.02) and L_d (r=0.77, slope=0.10, p=0.10) among the twelve reanalyses, if include the information of these patterns. Without considering spatial patterns of trend biases in variables, T_a trend biases show relative smaller correlation with R_s (r=0.32, slope=0.02, p>0.1), precipitation frequency (r=-0.51, slope=-0.02, p=0.09) and L_d (r=0.14, slope=0.02, p>0.1) among the reanalyses (Fig. 8). The same circumstances occur for the atmospheric water vapor (r=0.71, p=0.1) and cloud fraction (r=-0.74, p=0.09) if consider their spatial patterns (Figs. S19), and this relationship from cloud fraction is very similar to that from the R_s (Figs. 8 and S19). Over China's subregions, the trend biases in T_a show significant correlations with R_s (r=068 to 0.90, p<0.1), precipitation frequency (r=-0.55 to -0.94, p<0.1) and L_d (r=0.53 to 0.93, p<0.1) with the inclusion f spatial patterns among the reanalyses (Fig. S20). These results provide a novel view to investigate spatial relationship between trend biases in T_a and the relevant quantities among the reanalyses.

Discussion

In this section, we first examined the possible impact of data homogenization on the T_a trend. The T_a trends derived from the original dataset are almost higher than those from the homogenous dataset, especially over the North China Plain and Northwest China (Fig. 5 and Table 2). This homogenization primarily adjust the breakpoints in the time series (Wang, 2008) mainly due to station relocation and changes in instruments (Cao et al., 2016;Li et al., 2017;Wang, 2014), helps to objectively depict the T_a trend for assessment of modeled T_a trend and its spatial patterns in the reanalyses.

We found that the elevation difference between model and stations actually influence the T_a trend bias, but can not explain spatial pattern in the T_a trend bias (averaged r=0.11) (Fig. S21). Compared the same-grid models (NOAA 20CRv2c vs. NOAA 20CRv2, MERRA vs. MERRA2, NCEP-R1 vs. NCEP-R2 and ERA-20C vs.

ERA-20CM), we found the one statistically correlates with elevation difference but the other does not, which implies that this statistical correlation should not be physical significance. Besides, elevation difference does not change with time. Nevertheless, spatial patterns in normalized trends in T_a (excluding the impact of absolute value of temperature on the trends) are very near to those of the trends (Fig. S22), implying the impact of difference in absolute value of temperature due to the site-to-grid inconsistency can be neglected.

In reanalyses, only vegetation is included as climatology, but the vegetation has a growth trend in nature during the study period 1979-2010 over China (Fig. S23), which will positively enlarge the T_a trend biases due to the vegetation cooling effect (Zeng et al., 2017;Trigo et al., 2015). This effect is reflected by the negative spatial correlation (r=-0.26, p=0.00) between the inverted trend in NDVI and trend biases in T_a (Fig. S23). The vegetation growth would cool the near-surface air temperature by regulating surface roughness, surface conductivity, soil moisture and albedo to partition more available energy into latent heat fluxes and then formation of more precipitation (Shen et al., 2015;Spracklen et al., 2013), thereby inclusion of vegetation growth will have improved effect on the trend simulation (especially for the spatial pattern) of T_a in reanalyses through a more complete physical parameterizations above in reanalysis (Li et al., 2005;Dee and Todling, 2000;Trigo et al., 2015).

Due to the assimilation of surface air temperature, the ERA-Interim and JRA-55 exhibit a relatively skillful pattern with near-zero means (0.01 and 0.01 ℃/decade) and the smallest standard deviations (0.16 and 0.15 ℃/decade) of trend biases among the twelve reanalysis products, albeit being still evident pattern differences of 37.8% (standard deviation of trend bias/China-averaged Trend) (Figs. 5 and 8). Despite of no assimilation of surface air temperature, ERA-20CM also present a comparable pattern (mean of -0.04 ℃/decade and standard deviation of 0.15 ℃/decade, Figs. 5 and 8) to ERA-Interim and JRA-55, which implies a potential approach of multi-model ensemble forecast to this end. This advantage of multi-model ensemble forecast technique in ERA-20CM also perform better in the simulated pattern of trend biases in R_s (SD=1.84 W m^{-2}/decade, 171%), precipitation frequency (SD=2.78days/decade, 122%) and L_d (SD=1.25 W m^{-2}/decade, 82%) (Fig. 8).

We considered to which extent the ensemble assimilation technique can improve spatial patterns of the T_a trend bias in reanalyses. We found that this technique can explain the T_a trend biases over approximately 12% (8%) of grids for CERA-20C with 10 ensembles (NOAA 20CR2vc and NOAA 20CR2v with 56 ensembles) (Figs. 5l-n). However, the T_a trend biases over these grids were detected to be non-significant at the significance level of 0.05 for Student's *t*-test, implying that the ensemble assimilation technique can not explain spatial pattern of the T_a trend biases displayed in this study (in Figs. 5l-n).

To preliminarily discuss improvements of climate forecast models in reflecting patterns in climate trends, we compared spatial patterns of trend biases in R_s, precipitation frequency and L_d without direct observations assimilated. We can find that the climate forecast models, i.e., ERA-20C, ERA-20CM, CERA-20C, NOAA 20CRv2c and NOAA 20CRv2, perform better in pattern of trend biases in R_s (mean of

Atmos. Chem. Phys. Discuss., https://doi.org/10.5194/acp-2017-966
Manuscript under review for journal Atmos. Chem. Phys.
Discussion started: 22 December 2017

1.36 vs. 2.18 W m^{-2}/decade, SD of 2.04 vs. 2.71 W m^{-2}/decade), precipitation frequency (mean of 1.32 vs. -1.44 %/decade, SD of 3.57 vs. 6.14 %/decade) and L_d (mean of 0.12 vs. -0.85 W m^{-2}/decade, SD of 1.33 vs. 1.50 W m^{-2}/decade) than the NWP models, i.e., ERA-Interim, NCEP-R1, MERRA, JRA-55, NCEP-R2 and MERRA2 (Fig. 8). Besides, because the SST boundary condition freely evolved in CFSR, the patterns of trend biases in R_s, precipitation frequency and L_d in CFSR substantially differ from the other reanalyses.

We also considered whether spatial pattern of trend biases in T_a is altered by atmospheric circulations simulated by ERA-20CM ensembles. In ERA-20CM, the atmospheric circulations are controlled by pressure data with some influence from SSTs that partly mediate the influences of global forcings on the T_a trend. In ERA-20CM, probability distribution function of the T_a trend biases from outside the ensemble ranges incorporates that from Student's t-test at a significance level of 0.05 (Fig. 5k) has important implications that 1) the climate variability in model ensembles under the different realizations of SSTs and sea ice cover does not change the pattern of the T_a trend biases (Fig. 5k); 2) A Student's t-test exhibits a suitable ability to detect the significance of the T_a trend biases (Fig. 5k) for considering the effect of interannual variability on the trend.

4. Conclusions and Perspectives

Reanalyses have differences in T_a referenced to observations with a range of -10~10 ℃ over China, approximately 74% and 6% of which can be explained the site-to-grid elevation difference and the filtering error in spectral model elevation. This implies a fairly good skill in the simulation of climatology of T_a in the twelve reanalyses over China. Moreover, reanalyses roughly capture the interannual variability of T_a among the twelve reanalysis (median r=0.95). Reanalyses exhibit that T_a has consistently positive correlations with the R_s and L_d, and has negative correlations with precipitation frequency as those in observations, despite of having evident spatial patterns in their magnitudes over China.

The T_a exhibits a strong warming trend of 0.37 ℃/decade (p<0.05) from the observations and 0.22-0.48 ℃/decade (p<0.05) among the twelve reanalyses over China. In observation, approximately 87% of the observed T_a trend can be explained by greenhouse effect (i.e., trend in L_d, 65%), the precipitation frequency (29%) and R_s (-7%, due to the trend of -1.1 W·m^{-2}/decade) over China.

However, the trends biases in T_a from reanalyses to the observations display an evident spatial pattern (mean=-0.16~0.11 ℃/decade, SD=0.15-0.30 ℃/decade). The spatial patterns of the trends biases in reanalyzed T_a have significant correlations with those in R_s (maximum r =0.42, p<0.05), precipitation frequency (maximum r =-0.62, p<0.05) and L_d (maximum r =0.50, p<0.05). Over northern China, the trend biases in T_a (by order of -0.12 ℃/decade) primarily result from a combination of those in L_d (by order of -0.10 ℃/decade) and precipitation frequency (by order of 0.05 ℃/decade), with relatively small contribution from R_s (by order of -0.03 ℃/decade). Over southern China, the trend biases in T_a (by order of -0.07 ℃/decade) are regulated by the trend biases those in R_s (by order of 0.10 ℃/decade), L_d (by order of

Atmos. Chem. Phys. Discuss., https://doi.org/10.5194/acp-2017-966
Manuscript under review for journal Atmos. Chem. Phys.
Discussion started: 22 December 2017

-0.08 ℃/decade) and the precipitation frequency (by order of -0.06 ℃/decade).

If include information of spatial patterns, the simulated trend biases of T_a correlate well with those of precipitation frequency, R_s and L_d among the reanalyses (r=-0.83, 0.80 and 0.77, p<0.1), so they are for the atmospheric water vapor and cloud fraction (r=0.71 and -0.74, p<0.1). These results provide a novel view to investigate the spatial relationship between the trend biases in T_a and the relevant parameters among the twelve reanalyses.

From the observation, model and assimilation method, we comprehensively discussed their possible impact on the simulated biases in spatial pattern of the T_a trends. Overall, it's a challenge to produce a global or regional reanalysis suitable for region climate under the current strategy and to-do improvement. Based on the results above, some potential but challenging approaches arise to maximize regional climate signal component in the final reanalysis and robustly narrow the trend uncertainties:

1) As a pioneer, MERRA2 tried to incorporate time-varying aerosol loadings to improve regional warming over the North China Plain to some extent, so encourage to assimilate the accurate aerosol information and improve simulated skill of energy budget and partitioning, especially for regional surface incident solar radiation in the other reanalyses.

2) Make use of precipitation datasets with high temporal resolution from *in-situ* and satellite-based observations (Zhou and Wang, 2017a;Trenberth and Zhang, 2017;Dai et al., 2017) or the GPS water vapor (Bengtsson et al., 2003;Voosen, 2017;Poli et al., 2010) to dynamically constrain precipitation occurrence including

Atmos. Chem. Phys. Discuss., https://doi.org/10.5194/acp-2017-966
Manuscript under review for journal Atmos. Chem. Phys.
Discussion started: 22 December 2017

precipitation intensity and frequency (Qian et al., 2006;Trenberth et al., 2011;Bengtsson et al., 2007;Trenberth, 2004). This, in turn, will have more accurate representations of clouds and precipitation, especially their responses to climate change (Dai et al., 2017;Zhou and Wang, 2017b).

3) Produce forecast output using a perturbed physical ensemble like ERA-20CM to quantify the uncertainty associated with relevant parameterizations in reanalyses, due to impossibility to optimize all the biases to improve regional climate modeling. Meanwhile, careful ensemble design would probably yield useful information to improve model/assimilation and bias correction of observation by exploring interdependency among sources of errors. They would undoubtedly have additional benefit for further development pathways to the next generation of reanalyses.

4) Incorporate the true dynamics of land cover and use and improve the physical parameterizations such as the response of surface roughness, surface conductivity and albedo to regional climates, rather than constant type and fraction of vegetation as ERA-Interim (Zhou and Wang, 2016a), to improve the coupling of land-atmospheric interaction.

5) Implication from the spurious performance of freely evolved boundary conditions in CFSR, the homogeneous SST/sea ice should be reconstructed by bringing together many previous versions and new ARGO ocean observing network.

A next-generation reanalysis including global and regional reanalyses will have focus not only on short-term accuracy and long-term trends by assimilating *in-situ* observations, satellite radiances, and other remote observations, but also on their spatial patterns by incorporating or improving accurate representations of land surface conditions and processes within unified weather-climate coupled Earth systems, to advance the simulation of the land-atmosphere interactions for good skill in regional warming studies, so as for the detection and attribution of regional climate changes using various datasets and global/regional reanalyses widely included (Zhou et al., 2017b;Zhou and Wang, 2016d;Herring et al., 2016;Trenberth et al., 2015;Stott, 2016). Additionally, the uncertainties of regional warming could be ascertained by perturbed model physics ensembles with various equiprobable realizations of boundary conditions.

Acknowledgements This study was funded by the National Key R&D Program of China (2017YFA0603601), the National Natural Science Foundation of China (41525018). The latest observation datasets were obtained from the China Meteorological Administration (CMA, http://www.cma.gov.cn). Considerable gratitude is owed to several reanalysis working teams, including the European Centre for Medium-Range Weather Forecasts (ECMWF) for providing ERA-Interim, ERA-20C, ERA-20CM and CERA-20C data (http://www.ecmwf.int/); the Global Modeling and Assimilation Office (GMAO) at the NASA Goddard Space Flight Center for MERRA and MERRA2 data (http://gmao.gsfc.nasa.gov/); the NOAA Earth System Research Laboratory (ESRL) for NCEP-R1, NCEP-R2, CFSR NOAA 20CRv2 and NOAA 20CRv2c data (http://www.esrl.noaa.gov/); and the Climate Prediction Division of the Global Environment and Marine Department at the Japan

Meteorological Agency for JRA-55 data (http://jra.kishou.go.jp/). We thank the Expert Team on Climate Change Detection and Indices (ETCCDI) for the RHtestV4 package (http://etccdi.pacificclimate.org/software.shtml), the United States Geological Survey Earth Resources Observation and Science Data Center for GTOPO30 (http://edc.usgs.gov/products/elevation/gtopo30/gtopo30.html) and the working team for the Global Inventory Monitoring and Modeling System (GIMMS) project (https://ecocast.arc.nasa.gov/data/pub/gimms/). We thank Kevin E. Trenberth for his insightful suggestions.

Atmos. Chem. Phys. Discuss., https://doi.org/10.5194/acp-2017-966
Manuscript under review for journal Atmos. Chem. Phys.
Discussion started: 22 December 2017

References

Aarnes, O. J., Abdalla, S., Bidlot, J.-R., and Breivik, Ø.: Marine wind and wave height trends at different ERA-Interim forecast ranges, J. Clim., 28, 819-837, 10.1175/jcli-d-14-00470.1, 2015.

Andersson, E., Bauer, P., Beljaars, A., Chevallier, F., Holm, E., Janiskova, M., Kallberg, P., Kelly, G., Lopez, P., McNally, A., Moreau, E., Simmons, A. J., Thepaut, J. N., and Tompkins, A. M.: Assimilation and modeling of the atmospheric hydrological cycle in the ECMWF forecasting system, Bull. Am. Meteorol. Soc., 86, 387-402, 10.1175/bams-86-3-387, 2005.

Balsamo, G., Albergel, C., Beljaars, A., Boussetta, S., Brun, E., Cloke, H., Dee, D., Dutra, E., Muñoz-Sabater, J., Pappenberger, F., de Rosnay, P., Stockdale, T., and Vitart, F.: ERA-Interim/Land: a global land surface reanalysis data set, Hydrol. Earth Syst. Sci., 19, 389-407, 10.5194/hess-19-389-2015, 2015.

Bauer, P., Thorpe, A., and Brunet, G.: The quiet revolution of numerical weather prediction, Nature, 525, 47-55, 10.1038/nature14956, 2015.

Bengtsson, L., Kanamitsu, M., Kallberg, P., and Uppala, S.: FGGE research activities at ECMWF, Bull. Am. Meteorol. Soc., 63, 227-303, 1982a.

Bengtsson, L., Kanamitsu, M., Kallberg, P., and Uppala, S.: FGGE 4-dimensional data assimilation at ECMWF, Bull. Am. Meteorol. Soc., 63, 29-43, 1982b.

Bengtsson, L., and Shukla, J.: Integration of space and in situ observations to study global climate change, Bull. Am. Meteorol. Soc., 69, 1130-1143, 10.1175/1520-0477(1988)069<1130:iosais>2.0.co;2, 1988.

Bengtsson, L., Robinson, G., Anthes, R., Aonashi, K., Dodson, A., Elgered, G., Gendt, G., Gurney, R., Jietai, M., and Mitchell, C.: The use of GPS measurements for water vapor determination, Bull. Am. Meteorol. Soc., 84, 1249-1258, 2003.

Bengtsson, L., Hagemann, S., and Hodges, K. I.: Can climate trends be calculated from reanalysis data?, J Geophys Res-Atmos, 109, D11111, 10.1029/2004jd004536, 2004.

Bengtsson, L., Haines, K., Hodges, K. I., Arkin, P., Berrisford, P., Bougeault, P., Kallberg, P., Simmons, A. J., Uppala, S., Folland, C. K., Gordon, C., Rayner, N., Thorne, P. W., Jones, P., Stammer, D., and Vose, R. S.: The need for a dynamical climate reanalysis, Bull. Am. Meteorol. Soc., 88, 495-501, 10.1175/bams-88-4-495, 2007.

Betts, A. K., Hong, S.-Y., and Pan, H.-L.: Comparison of NCEP-NCAR reanalysis with 1987 FIFE data, Mon. Wea. Rev., 124, 1480-1498, 10.1175/1520-0493(1996)124<1480:connrw>2.0.co;2, 1996.

Atmos. Chem. Phys. Discuss., https://doi.org/10.5194/acp-2017-966
Manuscript under review for journal Atmos. Chem. Phys.
Discussion started: 22 December 2017

Atmospheric Chemistry and Physics Discussions

Betts, A. K., Viterbo, P., and Beljaars, A. C. M.: Comparison of the land-surface interaction in the ECMWF reanalysis model with the 1987 FIFE data, Mon. Wea. Rev., 126, 186-198, 10.1175/1520-0493(1998)126<0186:cotlsi>2.0.co;2, 1998.

Betts, A. K.: Understanding hydrometeorology using global models, Bull. Am. Meteorol. Soc., 85, 1673-1688, 10.1175/bams-85-11-1673, 2004.

Bilbao, J., and De Miguel, A. H.: Estimation of daylight downward longwave atmospheric irradiance under clear-sky and all-sky conditions, J. Appl. Meteor. Climatol., 46, 878-889, 2007.

Brunt, D.: Notes on radiation in the atmosphere. I, Q. J. Roy. Meteorol. Soc., 58, 389-420, 1932.

Cao, L., Zhu, Y., Tang, G., Yuan, F., and Yan, Z.: Climatic warming in China according to a homogenized data set from 2419 stations, Int. J. Climatol., 36, 4384-4392, 10.1002/joc.4639, 2016.

Cash, B. A., III, J. L. K., Adams, J., Altshuler, E., Huang, B., Jin, E. K., Manganello, J., Marx, L., and Jung, T.: Regional structure of the Indian summer monsoon in observations, reanalysis, and simulation, J. Clim., 28, 1824-1841, 10.1175/jcli-d-14-00292.1, 2015.

Chen, J., Del Genio, A. D., Carlson, B. E., and Bosilovich, M. G.: The spatiotemporal structure of twentieth-century climate variations in observations and reanalyses. Part I: Long-term trend, J. Clim., 21, 2611-2633, 2008.

Choi, M., Jacobs, J. M., and Kustas, W. P.: Assessment of clear and cloudy sky parameterizations for daily downwelling longwave radiation over different land surfaces in Florida, USA, Geophys. Res. Lett., 35, L20402, 2008.

Compo, G. P., Whitaker, J. S., Sardeshmukh, P. D., Matsui, N., Allan, R. J., Yin, X., Gleason, B. E., Vose, R. S., Rutledge, G., Bessemoulin, P., Brönnimann, S., Brunet, M., Crouthamel, R. I., Grant, A. N., Groisman, P. Y., Jones, P. D., Kruk, M. C., Kruger, A. C., Marshall, G. J., Maugeri, M., Mok, H. Y., Nordli, Ø., Ross, T. F., Trigo, R. M., Wang, X. L., Woodruff, S. D., and Worley, S. J.: The twentieth century reanalysis project, Q. J. Roy. Meteorol. Soc., 137, 1-28, 10.1002/qj.776, 2011.

Compo, G. P., Sardeshmukh, P. D., Whitaker, J. S., Brohan, P., Jones, P. D., and McColl, C.: Independent confirmation of global land warming without the use of station temperatures, Geophys. Res. Lett., 40, 3170-3174, 2013.

Cornes, R. C., and Jones, P. D.: How well does the ERA-Interim reanalysis replicate trends in extremes of surface temperature across Europe?, J Geophys Res-Atmos, 118, 10262-10276, 10.1002/jgrd.50799, 2013.

Dai, A., Wang, J., Thorne, P. W., Parker, D. E., Haimberger, L., and Wang, X. L.: A

Atmos. Chem. Phys. Discuss., https://doi.org/10.5194/acp-2017-966
Manuscript under review for journal Atmos. Chem. Phys.
Discussion started: 22 December 2017

new approach to homogenize daily radiosonde humidity data, J. Clim., 24, 965-991, 10.1175/2010jcli3816.1, 2011.

Dai, A., Rasmussen, R. M., Liu, C., Ikeda, K., and Prein, A. F.: A new mechanism for warm-season precipitation response to global warming based on convection-permitting simulations, Clim. Dyn., published online, 10.1007/s00382-017-3787-6, 2017.

Dee, D. P., and Da Silva, A. M.: Data assimilation in the presence of forecast bias, Q. J. Roy. Meteorol. Soc., 124, 269-295, 1998.

Dee, D. P., and Todling, R.: Data assimilation in the presence of forecast bias: The GEOS moisture analysis, Mon. Wea. Rev., 128, 3268-3282, 10.1175/1520-0493(2000)128<3268:daitpo>2.0.co;2, 2000.

Dee, D. P.: Bias and data assimilation, Q. J. Roy. Meteorol. Soc., 131, 3323-3343, 2005.

Dee, D. P., and Uppala, S.: Variational bias correction of satellite radiance data in the ERA-Interim reanalysis, Q. J. Roy. Meteorol. Soc., 135, 1830-1841, 10.1002/qj.493, 2009.

Dee, D. P., Källén, E., Simmons, A. J., and Haimberger, L.: Comments on "Reanalyses suitable for characterizing long-term trends", Bull. Am. Meteorol. Soc., 92, 65-70, 10.1175/2010BAMS3070.1, 2011a.

Dee, D. P., Uppala, S. M., Simmons, A. J., Berrisford, P., Poli, P., Kobayashi, S., Andrae, U., Balmaseda, M. A., Balsamo, G., Bauer, P., Bechtold, P., Beljaars, A. C. M., van de Berg, L., Bidlot, J., Bormann, N., Delsol, C., Dragani, R., Fuentes, M., Geer, A. J., Haimberger, L., Healy, S. B., Hersbach, H., Hólm, E. V., Isaksen, L., Kållberg, P., Köhler, M., Matricardi, M., McNally, A. P., Monge-Sanz, B. M., Morcrette, J. J., Park, B. K., Peubey, C., de Rosnay, P., Tavolato, C., Thépaut, J. N., and Vitart, F.: The ERA-Interim reanalysis: configuration and performance of the data assimilation system, Q. J. Roy. Meteorol. Soc., 137, 553-597, 10.1002/qj.828, 2011b.

Dee, D. P., Balmaseda, M., Balsamo, G., Engelen, R., Simmons, A. J., and Thépaut, J. N.: Toward a consistent reanalysis of the climate system, Bull. Am. Meteorol. Soc., 95, 1235-1248, 10.1175/bams-d-13-00043.1, 2014.

Desroziers, G., Berre, L., Chapnik, B., and Poli, P.: Diagnosis of observation, background and analysis‐error statistics in observation space, Q. J. Roy. Meteorol. Soc., 131, 3385-3396, 2005.

Dolinar, E. K., Dong, X., and Xi, B.: Evaluation and intercomparison of clouds, precipitation, and radiation budgets in recent reanalyses using satellite-surface observations, Clim. Dyn., 46, 2123-2144, 10.1007/s00382-015-2693-z, 2016.

Atmos. Chem. Phys. Discuss., https://doi.org/10.5194/acp-2017-966
Manuscript under review for journal Atmos. Chem. Phys.
Discussion started: 22 December 2017

Fang, J.-Y., and Yoda, K.: Climate and vegetation in China (I). Changes in the altitudinal lapse rate of temperature and distribution of sea level temperature, Ecol. Res., 3, 37-51, 1988.

Fujiwara, M., Wright, J. S., Manney, G. L., Gray, L. J., Anstey, J., Birner, T., Davis, S., Gerber, E. P., Harvey, V. L., Hegglin, M. I., Homeyer, C. R., Knox, J. A., Kruger, K., Lambert, A., Long, C. S., Martineau, P., Molod, A., Monge-Sanz, B. M., Santee, M. L., Tegtmeier, S., Chabrillat, S., Tan, D. G. H., Jackson, D. R., Polavarapu, S., Compo, G. P., Dragani, R., Ebisuzaki, W., Harada, Y., Kobayashi, C., McCarty, W., Onogi, K., Pawson, S., Simmons, A., Wargan, K., Whitaker, J. S., and Zou, C.-Z.: Introduction to the SPARC reanalysis intercomparison project (S-RIP) and overview of the reanalysis systems, Atmos. Chem. Phys., 17, 1417-1452, 10.5194/acp-17-1417-2017, 2017.

Gervais, M., Gyakum, J. R., Atallah, E., Tremblay, L. B., and Neale, R. B.: How well are the distribution and extreme values of daily precipitation over North America represented in the community climate system model? A comparison to reanalysis, satellite, and gridded station data, J. Clim., 27, 5219-5239, 10.1175/jcli-d-13-00320.1, 2014.

Gibson, J., Kållberg P, Uppala S, Nomura A, Hernandez A, and E., S.: ERA description, ECMWF. ERA-15 Project Report Series 1, European Centre for Medium-range Weather Forecasts, Reading, UK., 1997.

Golub, G. H., and Van Loan, C. F.: An analysis of the total least squares problem, SIAM J. Numer. Anal., 17, 883-893, 1980.

Heng, Z., Fu, Y., Liu, G., Zhou, R., Wang, Y., Yuan, R., Guo, J., and Dong, X.: A study of the distribution and variability of cloud water using ISCCP, SSM/I cloud product, and reanalysis datasets, J. Clim., 27, 3114-3128, 10.1175/jcli-d-13-00031.1, 2014.

Herring, S. C., Hoerling, M. P., Kossin, J. P., Peterson, T. C., and Stott, P. A.: Explaining extreme events of 2015 from a climate perspective, Bull. Am. Meteorol. Soc., 97, S1-S145, 2016.

Hersbach, H., Peubey, C., Simmons, A., Berrisford, P., Poli, P., and Dee, D.: ERA-20CM: a twentieth-century atmospheric model ensemble, Q. J. Roy. Meteorol. Soc., 141, 2350-2375, 10.1002/qj.2528, 2015.

Hines, K. M., Bromwich, D. H., and Marshall, G. J.: Artificial surface pressure trends in the NCEP-NCAR reanalysis over the southern ocean and Antarctica, J. Clim., 13, 3940-3952, 10.1175/1520-0442(2000)013<3940:asptit>2.0.co;2, 2000.

Hyk, W., and Stojek, Z.: Quantifying uncertainty of determination by standard additions and serial dilutions methods taking into account standard uncertainties in both axes, Anal. Chem., 85, 5933-5939, 2013.

Kalnay, E., Kanamitsu, M., Kistler, R., Collins, W., Deaven, D., Gandin, L., Iredell, M., Saha, S., White, G., and Woollen, J.: The NCEP/NCAR 40-year reanalysis project, Bull. Am. Meteorol. Soc., 77, 437-471, 1996.

Kanamitsu, M., Ebisuzaki, W., Woollen, J., Yang, S.-K., Hnilo, J. J., Fiorino, M., and Potter, G. L.: NCEP–DOE AMIP-II Reanalysis (R-2), Bull. Am. Meteorol. Soc., 83, 1631-1643, 10.1175/BAMS-83-11-1631, 2002.

Kidston, J., Frierson, D. M. W., Renwick, J. A., and Vallis, G. K.: Observations, simulations, and dynamics of jet stream variability and annular modes, J. Clim., 23, 6186-6199, 10.1175/2010jcli3235.1, 2010.

Kobayashi, S., Ota, Y., Harada, Y., Ebita, A., Moriya, M., Onoda, H., Onogi, K., Kamahori, H., Kobayashi, C., Endo, H., Miyaoka, K., and Takahashi, K.: The JRA-55 reanalysis: general specifications and basic characteristics, J. Meteorol. Soc. Jpn., 93, 5-48, 10.2151/jmsj.2015-001, 2015.

Lahoz, W. A., and Schneider, P.: Data assimilation: making sense of Earth Observation, Front.Environ.Sci., 2, 1-28, 10.3389/fenvs.2014.00016, 2014.

Laloyaux, P., Balmaseda, M., Dee, D., Mogensen, K., and Janssen, P.: A coupled data assimilation system for climate reanalysis, Q. J. Roy. Meteorol. Soc., 142, 65-78, 10.1002/qj.2629, 2016.

Li, H. B., Robock, A., Liu, S. X., Mo, X. G., and Viterbo, P.: Evaluation of reanalysis soil moisture simulations using updated Chinese soil moisture observations, J. Hydrometeorol., 6, 180-193, 10.1175/jhm416.1, 2005.

Li, Q., Zhang, L., Xu, W., Zhou, T., Wang, J., Zhai, P., and Jones, P.: Comparisons of Time Series of Annual Mean Surface Air Temperature for China since the 1900s: Observations, Model Simulations, and Extended Reanalysis, Bull. Am. Meteorol. Soc., 98, 699-711, 10.1175/bams-d-16-0092.1, 2017.

Li, Y., Zeng, Z. Z., Zhao, L., and Piao, S. L.: Spatial patterns of climatological temperature lapse rate in mainland China: A multi-time scale investigation, J Geophys Res-Atmos, 120, 2661-2675, Doi 10.1002/2014jd022978, 2015.

Lin, R., Zhou, T., and Qian, Y.: Evaluation of global monsoon precipitation changes based on five reanalysis datasets, J. Clim., 27, 1271-1289, doi:10.1175/JCLI-D-13-00215.1, 2014.

Lindsay, R., Wensnahan, M., Schweiger, A., and Zhang, J.: Evaluation of seven different atmospheric reanalysis products in the Arctic, J. Clim., 27, 2588-2606, 10.1175/jcli-d-13-00014.1, 2014.

Ma, L., Zhang, T., Li, Q., Frauenfeld, O. W., and Qin, D.: Evaluation of ERA-40, NCEP-1, and NCEP-2 reanalysis air temperatures with ground-based measurements in China, J. Geophys. Res. D Atmos., 113, D15115, 10.1029/2007JD009549, 2008.

Mao, J., Shi, X., Ma, L., Kaiser, D. P., Li, Q., and Thornton, P. E.: Assessment of reanalysis daily extreme temperatures with china's homogenized historical dataset during 1979-2001 using probability density functions, J. Clim., 23, 6605-6623, 10.1175/2010jcli3581.1, 2010.

Mitas, C. M., and Clement, A.: Recent behavior of the Hadley cell and tropical thermodynamics in climate models and reanalyses, Geophys. Res. Lett., 33, L01810, 10.1029/2005gl024406, 2006.

Nguyen, H., Evans, A., Lucas, C., Smith, I., and Timbal, B.: The Hadley circulation in reanalyses: climatology, variability, and change, J. Clim., 26, 3357-3376, 10.1175/jcli-d-12-00224.1, 2013.

Niznik, M. J., and Lintner, B. R.: Circulation, moisture, and precipitation relationships along the south Pacific convergence zone in reanalyses and CMIP5 models, J. Clim., 26, 10174-10192, 10.1175/jcli-d-13-00263.1, 2013.

Onogi, K., Tslttsui, J., Koide, H., Sakamoto, M., Kobayashi, S., Hatsushika, H., Matsumoto, T., Yamazaki, N., Kaalhori, H., Takahashi, K., Kadokura, S., Wada, K., Kato, K., Oyama, R., Ose, T., Mannoji, N., and Taira, R.: The JRA-25 reanalysis, J. Meteorol. Soc. Jpn., 85, 369-432, Doi 10.2151/Jmsj.85.369, 2007.

Parker, W. S.: Reanalyses and observations: What's the difference?, Bull. Am. Meteorol. Soc., 97, 1565-1572, 10.1175/bams-d-14-00226.1, 2016.

Peña, M., and Toth, Z.: Estimation of analysis and forecast error variances, Tellus A, 66, 21767, 2014.

Piao, S. L., Yin, L., Wang, X. H., Ciais, P., Peng, S. S., Shen, Z. H., and Seneviratne, S. I.: Summer soil moisture regulated by precipitation frequency in China, Environ. Res. Lett., 4, 044012, 10.1088/1748-9326/4/4/044012, 2009.

Pitman, A. J., and Perkins, S. E.: Global and regional comparison of daily 2-m and 1000-hpa maximum and minimum temperatures in three global reanalyses, J. Clim., 22, 4667-4681, 10.1175/2009jcli2799.1, 2009.

Poli, P., Healy, S. B., and Dee, D. P.: Assimilation of Global Positioning System radio occultation data in the ECMWF ERA-Interim reanalysis, Q. J. Roy. Meteorol. Soc., 136, 1972-1990, 10.1002/qj.722, 2010.

Poli, P., Hersbach, H., Dee, D. P., Berrisford, P., Simmons, A. J., Vitart, F., Laloyaux, P., Tan, D. G. H., Peubey, C., Thépaut, J.-N., Trémolet, Y., Hólm, E. V., Bonavita, M., Isaksen, L., and Fisher, M.: ERA-20C: An atmospheric reanalysis of the twentieth century, J. Clim., 29, 4083-4097, doi:10.1175/JCLI-D-15-0556.1, 2016.

Atmos. Chem. Phys. Discuss., https://doi.org/10.5194/acp-2017-966
Manuscript under review for journal Atmos. Chem. Phys.
Discussion started: 22 December 2017

Atmospheric Chemistry and Physics
Open Access
Discussions

Qian, T. T., Dai, A., Trenberth, K. E., and Oleson, K. W.: Simulation of global land surface conditions from 1948 to 2004. Part I: Forcing data and evaluations, J. Hydrometeorol., 7, 953-975, Doi 10.1175/Jhm540.1, 2006.

Reed, B. C.: Linear least‐squares fits with errors in both coordinates, Am. J. Phys., 57, 642-646, 1989.

Reichle, R. H., Koster, R. D., De Lannoy, G. J. M., Forman, B. A., Liu, Q., Mahanama, S. P. P., and Touré, A.: Assessment and enhancement of MERRA land surface hydrology estimates, J. Clim., 24, 6322-6338, 10.1175/JCLI-D-10-05033.1, 2011.

Reichle, R. H., Liu, Q., Koster, R. D., Draper, C. S., Mahanama, S. P. P., and Partyka, G. S.: Land surface precipitation in MERRA-2, J. Clim., 30, 1643-1664, 10.1175/jcli-d-16-0570.1, 2017.

Reuten, C., Moore, R. D., and Clarke, G. K. C.: Quantifying differences between 2-m temperature observations and reanalysis pressure-level temperatures in northwestern North America, J. Appl. Meteor. Climatol., 50, 916-929, 10.1175/2010jamc2498.1, 2011.

Rienecker, M. M., Suarez, M. J., Gelaro, R., Todling, R., Bacmeister, J., Liu, E., Bosilovich, M. G., Schubert, S. D., Takacs, L., Kim, G.-K., Bloom, S., Chen, J., Collins, D., Conaty, A., da Silva, A., Gu, W., Joiner, J., Koster, R. D., Lucchesi, R., Molod, A., Owens, T., Pawson, S., Pegion, P., Redder, C. R., Reichle, R., Robertson, F. R., Ruddick, A. G., Sienkiewicz, M., and Woollen, J.: MERRA: NASA's Modern-Era Retrospective Analysis for Research and Applications, J. Clim., 24, 3624-3648, 10.1175/JCLI-D-11-00015.1, 2011.

Ryan, T. P.: Modern regression methods, John Wiley & Sons, 2008.

Saha, S., Moorthi, S., Pan, H. L., Wu, X. R., Wang, J. D., Nadiga, S., Tripp, P., Kistler, R., Woollen, J., Behringer, D., Liu, H. X., Stokes, D., Grumbine, R., Gayno, G., Wang, J., Hou, Y. T., Chuang, H. Y., Juang, H. M. H., Sela, J., Iredell, M., Treadon, R., Kleist, D., Van Delst, P., Keyser, D., Derber, J., Ek, M., Meng, J., Wei, H. L., Yang, R. Q., Lord, S., Van den Dool, H., Kumar, A., Wang, W. Q., Long, C., Chelliah, M., Xue, Y., Huang, B. Y., Schemm, J. K., Ebisuzaki, W., Lin, R., Xie, P. P., Chen, M. Y., Zhou, S. T., Higgins, W., Zou, C. Z., Liu, Q. H., Chen, Y., Han, Y., Cucurull, L., Reynolds, R. W., Rutledge, G., and Goldberg, M.: The NCEP climate forecast system reanalysis, Bull. Am. Meteorol. Soc., 91, 1015-1057, 10.1175/2010BAMS3001.1, 2010.

Schoeberl, M. R., Dessler, A. E., and Wang, T.: Simulation of stratospheric water vapor and trends using three reanalyses, Atmos. Chem. Phys., 12, 6475-6487, 10.5194/acp-12-6475-2012, 2012.

Shen, M., Piao, S., Jeong, S.-J., Zhou, L., Zeng, Z., Ciais, P., Chen, D., Huang, M., Jin,

Atmos. Chem. Phys. Discuss., https://doi.org/10.5194/acp-2017-966
Manuscript under review for journal Atmos. Chem. Phys.
Discussion started: 22 December 2017

C.-S., and Li, L. Z.: Evaporative cooling over the Tibetan Plateau induced by vegetation growth, Proc. Nat. Acad. Sci. U.S.A., 112, 9299-9304, 2015.

Simmonds, I., and Keay, K.: Mean Southern Hemisphere extratropical cyclone behavior in the 40-year NCEP-NCAR reanalysis, J. Clim., 13, 873-885, 10.1175/1520-0442(2000)013<0873:mshecb>2.0.co;2, 2000.

Simmons, A. J., Willett, K. M., Jones, P. D., Thorne, P. W., and Dee, D. P.: Low-frequency variations in surface atmospheric humidity, temperature, and precipitation: Inferences from reanalyses and monthly gridded observational data sets, J. Geophys. Res. D Atmos., 115, D01110, 10.1029/2009JD012442, 2010.

Siswanto, S., Oldenborgh, G. J., Schrier, G., Jilderda, R., and Hurk, B.: Temperature, extreme precipitation, and diurnal rainfall changes in the urbanized Jakarta city during the past 130 years, Int. J. Climatol., 36, 3207-3225, 2015.

Spracklen, D. V., Arnold, S. R., and Taylor, C. M.: Observations of increased tropical rainfall preceded by air passage over forests, Nature, 494, 390-390, 10.1038/nature11904, 2013.

Stott, P.: How climate change affects extreme weather events, Science, 352, 1517-1518, 10.1126/science.aaf7271, 2016.

Tang, W.-J., Yang, K., Qin, J., Cheng, C., and He, J.: Solar radiation trend across China in recent decades: a revisit with quality-controlled data, Atmos. Chem. Phys., 11, 393-406, 2011.

Tellinghuisen, J.: Least-squares analysis of data with uncertainty in x and y: A Monte Carlo methods comparison, Chemom. Intell. Lab. Syst., 103, 160-169, 2010.

Thorne, P., and Vose, R.: Reanalyses suitable for characterizing long-term trends: Are they really achievable?, Bull. Am. Meteorol. Soc., 91, 353-361, 2010.

Trenberth, K. E., and Olson, J. G.: An evaluation and intercomparison of global analyses from the National-Meteorological-Center and the European-Centre-for-Medium-Range-Weather-Forecasts, Bull. Am. Meteorol. Soc., 69, 1047-1057, Doi 10.1175/1520-0477(1988)069<1047:Aeaiog>2.0.Co;2, 1988.

Trenberth, K. E.: Climatology - Rural land-use change and climate, Nature, 427, 213-213, 10.1038/427213a, 2004.

Trenberth, K. E., Koike, T., and Onogi, K.: Progress and prospects for reanalysis for weather and climate, Eos Trans. Am. Geophys. Union, 89, 234-235, 10.1029/2008EO260002, 2008.

Trenberth, K. E., Fasullo, J. T., and Mackaro, J.: Atmospheric Moisture Transports from Ocean to Land and Global Energy Flows in Reanalyses, J. Clim., 24, 4907-4924, 10.1175/2011JCLI4171.1, 2011.

Trenberth, K. E., Fasullo, J. T., and Shepherd, T. G.: Attribution of climate extreme events, Nature Clim. Change, 5, 725-730, 10.1038/nclimate2657, 2015.

Trenberth, K. E., and Zhang, Y.: “How often does it really rain?”, Bull. Am. Meteorol. Soc., published online, 10.1175/bams-d-17-0107.1, 2017.

Trigo, I., Boussetta, S., Viterbo, P., Balsamo, G., Beljaars, A., and Sandu, I.: Comparison of model land skin temperature with remotely sensed estimates and assessment of surface‐atmosphere coupling, J. Geophys. Res. D Atmos., 120, D023812, 10.1002/2015JD023812, 2015.

Tsidu, G. M.: High-resolution monthly rainfall database for Ethiopia: Homogenization, reconstruction, and gridding, J. Clim., 25, 8422-8443, 10.1175/jcli-d-12-00027.1, 2012.

Uppala, S. M., KÅllberg, P. W., Simmons, A. J., Andrae, U., Bechtold, V. D. C., Fiorino, M., Gibson, J. K., Haseler, J., Hernandez, A., Kelly, G. A., Li, X., Onogi, K., Saarinen, S., Sokka, N., Allan, R. P., Andersson, E., Arpe, K., Balmaseda, M. A., Beljaars, A. C. M., Berg, L. V. D., Bidlot, J., Bormann, N., Caires, S., Chevallier, F., Dethof, A., Dragosavac, M., Fisher, M., Fuentes, M., Hagemann, S., Hólm, E., Hoskins, B. J., Isaksen, L., Janssen, P. A. E. M., Jenne, R., McNally, A. P., Mahfouf, J. F., Morcrette, J. J., Rayner, N. A., Saunders, R. W., Simon, P., Sterl, A., Trenberth, K. E., Untch, A., Vasiljevic, D., Viterbo, P., and Woollen, J.: The ERA-40 re-analysis, Q. J. Roy. Meteorol. Soc., 131, 2961-3012, 10.1256/qj.04.176, 2005.

Venema, V., Mestre, O., Aguilar, E., Auer, I., Guijarro, J., Domonkos, P., Vertacnik, G., Szentimrey, T., Stepanek, P., and Zahradnicek, P.: Benchmarking homogenization algorithms for monthly data, Clim. Past, 8, 89-115, 2012.

Voosen, P.: GPS satellites yield space weather data, Science, 355, 443-443, 10.1126/science.355.6324.443, 2017.

Wang, A., and Zeng, X.: Evaluation of multireanalysis products with in situ observations over the Tibetan Plateau, J. Geophys. Res. D Atmos., 117, D05102, 10.1029/2011JD016553, 2012.

Wang, K., and Liang, S.: Global atmospheric downward longwave radiation over land surface under all‐sky conditions from 1973 to 2008, J. Geophys. Res. D Atmos., 114, D19101, 2009.

Wang, K., Dickinson, R., Wild, M., and Liang, S.: Atmospheric impacts on climatic variability of surface incident solar radiation, Atmos. Chem. Phys., 12, 9581-9592, 2012.

Wang, K., and Dickinson, R. E.: Global atmospheric downward longwave radiation at the surface from ground-based observations, satellite retrievals, and reanalyses, Rev. Geophys., 51, 150-185, 10.1002/rog.20009, 2013.

Wang, K.: Measurement biases explain discrepancies between the observed and simulated decadal variability of surface incident solar radiation, Sci. Rep., 4, 6144, 10.1038/srep06144, 2014.

Wang, K. C., Ma, Q., Li, Z. J., and Wang, J. K.: Decadal variability of surface incident solar radiation over China: Observations, satellite retrievals, and reanalyses, J Geophys Res-Atmos, 120, 6500-6514, 10.1002/2015JD023420, 2015.

Wang, X., and Wang, K.: Homogenized variability of radiosonde-derived atmospheric boundary layer height over the global land surface from 1973 to 2014, J. Clim., 29, 6893-6908, doi:10.1175/JCLI-D-15-0766.1, 2016.

Wang, X. L., Wen, Q. H., and Wu, Y.: Penalized maximal t test for detecting undocumented mean change in climate data series, J. Appl. Meteor. Climatol., 46, 916-931, 2007.

Wang, X. L.: Penalized maximal F test for detecting undocumented mean shift without trend change, J. Atmos. Oceanic Technol., 25, 368-384, 2008.

Wang, X. L., Chen, H., Wu, Y., Feng, Y., and Pu, Q.: New techniques for the detection and adjustment of shifts in daily precipitation data series, J. Appl. Meteor. Climatol., 49, 2416-2436, 2010.

Wang, X. L., and Feng, Y.: RHtestsV4 user manual, Atmospheric Science and Technology Directorate, Science and Technology Branch, Environment Canada. 28 pp. available at http://etccdi.pacificclimate.org/software.shtml, 2013.

Wu, C., Chen, J. M., Pumpanen, J., Cescatti, A., Marcolla, B., Blanken, P. D., Ardö, J., Tang, Y., Magliulo, V., and Georgiadis, T.: An underestimated role of precipitation frequency in regulating summer soil moisture, Environ. Res. Lett., 7, 024011, 2012.

Xu, J., and Powell, A. M., Jr.: Uncertainty of the stratospheric/tropospheric temperature trends in 1979-2008: multiple satellite MSU, radiosonde, and reanalysis datasets, Atmos. Chem. Phys., 11, 10727-10732, 10.5194/acp-11-10727-2011, 2011.

Yang, K., Koike, T., and Ye, B.: Improving estimation of hourly, daily, and monthly solar radiation by importing global data sets, Agr. Forest Meteorol., 137, 43-55, 10.1016/j.agrformet.2006.02.001, 2006.

York, D., Evensen, N. M., Martínez, M. L., and Delgado, J. D. B.: Unified equations for the slope, intercept, and standard errors of the best straight line, Am. J. Phys., 72, 367-375, 10.1119/1.1632486, 2004.

You, Q., Kang, S., Pepin, N., Flügel, W.-A., Yan, Y., Behrawan, H., and Huang, J.:

Relationship between temperature trend magnitude, elevation and mean temperature in the Tibetan Plateau from homogenized surface stations and reanalysis data, Global Planet. Change, 71, 124-133, 10.1016/j.gloplacha.2010.01.020, 2010.

Zeng, Z., Piao, S., Li, L. Z., Zhou, L., Ciais, P., Wang, T., Li, Y., Lian, X., Wood, E. F., and Friedlingstein, P.: Climate mitigation from vegetation biophysical feedbacks during the past three decades, Nature Clim. Change, 7, 432-436, 2017.

Zhao, T., Guo, W., and Fu, C.: Calibrating and evaluating reanalysis surface temperature error by topographic correction, J. Clim., 21, 1440-1446, 10.1175/2007jcli1463.1, 2008.

Zhou, C., and Wang, K.: Evaluation of surface fluxes in ERA-Interim using flux tower data, J. Clim., 29, 1573-1582, 10.1175/JCLI-D-15-0523.1, 2016a.

Zhou, C., and Wang, K.: Land surface temperature over global deserts: means, variability and trends, J. Geophys. Res. D Atmos., 121, 2016JD025410, 10.1002/2016JD025410, 2016b.

Zhou, C., and Wang, K.: Biological and environmental controls on evaporative fractions at ameriflux sites, J. Appl. Meteor. Climatol., 55, 145-161, 10.1175/JAMC-D-15-0126.1, 2016c.

Zhou, C., and Wang, K.: Spatiotemporal divergence of the warming hiatus over land based on different definitions of mean temperature, Sci. Rep., 6, 31789, 10.1038/srep31789, 2016d.

Zhou, C., and Wang, K.: Contrasting daytime and nighttime precipitation variability between observations and eight reanalysis products from 1979 to 2014 in China, J. Clim., 30, 6443-6464, 10.1175/JCLI-D-16-0702.1, 2017a.

Zhou, C., and Wang, K.: Quantifying the sensitivity of precipitation to the long-term warming trend and interannual-decadal variation of surface air temperature over China, J. Clim., 30, 3687-3703, 10.1175/jcli-d-16-0515.1, 2017b.

Zhou, C., Wang, K., and Ma, Q.: Evaluation of eight current reanalyses in simulating land surface temperature from 1979 to 2003 in China, J. Clim., 30, 7379-7398, 10.1175/jcli-d-16-0903.1, 2017a.

Zhou, C., Wang, K., and Qi, D.: Attribution of the July 2016 extreme precipitation event over China's Wuhan, Bull. Am. Meteorol. Soc., in press, 2017b.

Table 1. Summarized information on the twelve reanalysis products, including institution, model resolution, assimilation system, assimilated surface observation associated with surface air temperature, sea ice/SST (sea surface temperature) and GHGs boundary condition. The number in the parentheses of Column Model Name is the year for the version of forecast model. More details for each product can be found in the associated reference.

Reanalysis	Institution	Model Name	Model Resolution	Period	Assimilation System
ERA-Interim	ECMWF	IFS version Cy31r2 (2007)	T255 ~80 km, 60 levels	1979 onwards	4D-VAR
JRA-55	JMA	JMA operational numerical weather precidition system (2009)	T319 ~55 km, 60 levels	1958-2013	4D-VAR
NCEP-R1	NCEP/NCAR	NCEP operational numerical weather precidition system (1995)	T62 ~210 km, 28 levels	1948 onwards	3D-VAR
NCEP-R2	NCEP/DOE	Modified NCEP-R1 model (1998)	T62 ~210 km, 28 levels	1979 onwards	3D-VAR
MERRA	NASA/GMAO	An GEOS-5.0.2 atmospheric general circulation model (2008)	0.5 °× 0.667 °~55 km, 72 levels	1979 onwards	3D-VAR with incremental update (GEOS IAU)
MERRA-2	NASA/GMAO	The updated model of GEOS-5.12.4 as MERRA and its land version similar to MERRA land (2015)	0.5 °× 0.625 °~55 km, 72 levels	1980 onwards	3D-VAR with incremental update (GEOS IAU)
ERA-20C	ECMWF	IFS version Cy38r1 (2012), coupled atmosphere-land-ocean -waves system	T159 ~125 km, 91 levels	1900-2010	4D-VAR
ERA-20CM	ECMWF	The similar model as ERA-20C (2012)	T159 ~125 km, 91 levels	1900-2010	4D-VAR
CERA-20C	ECMWF	IFS version Cy41r2 (2016), coupled atmosphere-ocean-land-waves-sea ice system	T159 ~125 km, 91 levels	1901-2010	CERA Ensemble Assimilation technique
NOAA 20CRv2c	NOAA/ESRL PSD	NCEP GFS (2008), an updated version of NCEP's CFS, coupled atmosphere-land model	T62 ~210 km, 28 levels	1851-2014	Ensemble Kalman Filter
NOAA 20CRv2	NOAA/ESRL PSD	The same model as NOAA 20CRv2c (2008)	T62 ~210 km, 28 levels	1871-2012	Ensemble Kalman Filter
CFSR	NCEP	NCEP Climate Forecast System (CFS) (2011), coupled atmosphere-ocean-land-sea ice model	T382 ~38 km, 64 levels	1979-2010	3D-VAR

Table 1. Continued at right column.

Related Assimilated Surface Observations	Sea Ice and SST	GHGs-forcing	Reference
1) Assimilating in-situ observations of land surface temperature/pressure/relative humidity and upper air temperatures/wind/specific humidity; 2) Assimilating rain-affected SSM/I radiances via the 1D+4D-Var approach.	A changing suite of SST and sea ice from the observations and the NCEP	Interpolation by 1.6 ppmv/year from 353 ppmv of global mean CO_2 in 1990	(Dee et al., 2011b)
Assimilating all available conventional and satellite observations	In-situ observation-based estimate of the COBE SST and sea ice	The same as CMIP5	(Kobayashi et al., 2015)
1) Initiated with weather observations from ships, planes, station data, satellite observations and many more; 2) No assimilation of surface air temperature 3) Using observed precipitation to nudge soil moisture; 4) no information on aerosol.	Reynolds SST for 1982 on and the UKMO GISST for earlier period; Sea Ice from SMMR/SSMI	Constant global mean CO_2, 330 ppmv and no other trace gases	(Kalnay et al., 1996)
1) Assimilation errors were corrected and a better version of the model was used; 2) No assimilation of surface air temperature; 3) no information on aerosol.	AMIP-II prescribed	Constant global mean CO_2, 350 ppmv and no other trace gases	(Kanamitsu et al., 2002)
1) Neither MERRA nor MERRA-2 assimilated surface meteorology station data over land including surface air temperature and relative humidity. 2) The radiosondes do provide some low level observations.	Reynolds SST prescribed	The same as CMIP5	(Rienecker et al., 2011)
1) Assimilating newer observations (not available to MERRA) after the 2010s 2) Assimilating aerosol observations from MODIS and AERONET over land after 2000s and GOCART model-derived aerosol before 2000s 3) Assimilating observation-corrected precipitation to correct model-generated precipitation before reaching the land surface	AMIP-II and Reynolds SST	The same as CMIP5	(Reichle et al., 2017)
1) Assimilating surface pressures from the International Surface Pressure Databank v3.2.6 and ICOADS v 2.5.1, and surface winds over the oceans from ICOADSv2.5.1; 2) Using monthly climatology of aerosol from CMIP5; 3) Including radiative forcings/land surface parameters from CMIP5.	SST/sea-ice from HadISST2.1.0.0	The same as CMIP5	(Poli et al., 2016)
Assimilating no data and including radiative forcings/land surface parameters from CMIP5	SST/sea-ice realizations from HadISST2.1.0.0 used in 10 members	The same as CMIP5	(Hersbach et al., 2015)
1) Assimilating surface and mean sea level pressures from ISPDv3.2.6 and ICOADSv2.5.1, and surface marine winds from ICOADSv2.5.1 2) Assimilating no data in the land, wave and sea-ice components, but the use of the coupled model ensures a dynamically consistent Earth system estimate at each time step.	SST from the HadISST2.1.0.0	The same as CMIP5	(Laloyaux et al., 2016)
Assimilating only surface pressure and sea level pressure at each time step	SST from HadISST1.1 and sea ice from the COBE-SST	Monthly 15°gridded estimation of CO_2 from WMO observation	(Compo et al., 2011)
The same as NOAA 20CRv2c	SST/sea-ice from HadISST1.1	Monthly 15°gridded estimation of CO_2 from WMO observation	(Compo et al., 2011)
1) Assimilating all available conventional and satellite observations, but no assimilation of land surface air temperature 2) The atmospheric model contained observed variations in carbon dioxide (CO_2) together with changes in aerosols; 3) Using observation-corrected precipitation to force the land surface analysis	generated by coupled ocean-sea ice models, evolving freely during the 6-h coupled model integration	Monthly 15°gridded estimation of CO_2 from WMO observation	(Saha et al., 2010)

Table 2. Difference (unit: ℃) relative to homogenous observations and Trend (unit: ℃/decade) in surface air temperature (T_a) from 1979 to 2010 over China and its seven subregions. The bold and italic bold fonts indicate a two-tailed Student's *t*-test with a significance level of 0.05 and 0.1, respectively.

Regions	China		Tibetan Plateau		Northwest China		Loess Plateau		Middle China		Northeast China		North China Plain		Southeast China	
	Diff.	Trend	Diff.	Trend	Diff.	Trend	Diff.	Trend	Diff.	Trend	Diff.	Trend	Diff.	Trend	Diff.	Trend
ERA-Interim	-0.87	**0.38**	-3.49	**0.33**	-1.82	**0.37**	-0.32	**0.50**	-1.19	**0.28**	-0.03	**0.42**	-0.02	**0.45**	-0.03	**0.37**
NCEP-R1	-2.56	**0.23**	-6.80	0.11	-4.45	**0.39**	-1.77	**0.21**	-2.91	**0.23**	-1.28	**0.27**	-1.21	**0.23**	-1.33	**0.22**
MERRA	-0.48	**0.25**	-3.48	**0.33**	0.95	0.14	1.14	0.09	-1.35	**0.12**	-0.22	**0.52**	0.67	**0.26**	-0.27	**0.24**
JRA-55	-1.10	**0.38**	-3.49	**0.42**	-1.70	**0.39**	-0.58	**0.52**	-1.61	**0.30**	-0.25	**0.37**	-0.26	**0.41**	-0.50	**0.34**
NCEP-R2	-2.10	**0.25**	-5.76	-0.07	-4.29	**0.58**	-1.33	0.10	-2.80	**0.20**	-0.51	**0.36**	-0.38	**0.23**	-1.14	**0.36**
MERRA2	-0.91	**0.28**	-3.41	**0.35**	0.34	**0.32**	0.12	**0.19**	-1.35	**0.23**	-0.73	**0.41**	-0.24	0.18	-0.64	**0.25**
ERA-20C	-1.42	**0.29**	-6.56	**0.33**	-1.95	**0.31**	0.03	0.21	-2.01	**0.35**	-0.19	**0.32**	1.05	0.19	-0.47	**0.28**
ERA-20CM	-1.48	**0.32**	-5.93	**0.28**	-1.39	**0.38**	-0.36	**0.33**	-2.13	**0.27**	-0.23	**0.41**	-0.31	**0.34**	-0.51	**0.29**
CERA-20C	-2.06	**0.34**	-7.00	**0.41**	-2.15	**0.38**	-0.78	**0.36**	-2.59	**0.34**	-0.76	**0.43**	-0.40	0.19	-1.20	**0.29**
NOAA 20CRv2c	-0.28	**0.22**	-2.75	**0.39**	-0.01	**0.28**	1.62	0.16	-1.68	**0.18**	-0.16	0.11	1.06	0.15	0.18	**0.22**
NOAA 20CRv2	-0.32	**0.24**	-2.78	**0.33**	-0.01	**0.29**	1.48	0.20	-1.77	**0.19**	-0.07	0.25	0.97	0.21	0.12	**0.19**
CFSR	-1.74	**0.48**	-5.09	**0.46**	-1.03	**0.44**	-0.25	**0.40**	-2.91	**0.37**	-0.49	**0.67**	-0.37	**0.47**	-1.58	**0.51**
Obs-raw	0.03	**0.40**	0.03	**0.46**	0.09	**0.44**	0.01	**0.52**	0.05	**0.30**	0.00	**0.40**	0.05	**0.42**	0.03	**0.36**
Obs-homo		**0.37**		**0.44**		**0.36**		**0.50**		**0.24**		**0.41**		**0.38**		**0.33**

Table 3. Spatial pattern correlation (unit: 1) of three groups: partial relationships, trends and simulated trend biases of surface air temperature (T_a) against surface incident solar radiation (R_s), precipitation frequency (PF) and surface downward longwave radiation (L_d). The bold and italic bold fonts indicate a two-tailed Student's *t*-test with a significance level of 0.05 and 0.1, respectively.

Pattern Correlation	Partial Relationship						Trend				Trend Bias		
	(T_a, R_s)		(T_a, PF)		(T_a, L_d)		(T_a, T_a)	(T_a, R_s)	(T_a, PF)	(T_a, L_d)	(T_a, R_s)	(T_a, PF)	(T_a, L_d)
	Corr.	Slope	Corr.	Slope	Corr.	Slope							
ERA-Interim	**0.29**	0.01	0.03	**0.31**	**0.21**	**0.25**	**0.47**	**-0.11**	-0.04	**0.33**	**0.26**	**-0.12**	**0.10**
NCEP-R1	**0.30**	***0.06***	**0.18**	**0.30**	**0.36**	0.00	0.02	**-0.36**	-0.02	**0.62**	-0.03	-0.04	**0.43**
MERRA	**0.29**	0.06	**0.13**	**0.39**	0.05	**0.20**	**0.21**	**0.66**	**-0.81**	**-0.53**	**0.42**	**-0.62**	-0.05
JRA-55	**0.35**	**0.21**	**0.22**	**0.16**	**0.29**	**0.27**	**0.54**	**-0.33**	**0.31**	**0.57**	0.00	**0.14**	**0.29**
NCEP-R2	**0.22**	0.03	**0.20**	**0.36**	**0.27**	0.04	**-0.08**	**0.18**	**-0.29**	**0.28**	**0.15**	**-0.14**	**0.35**
MERRA2	**0.13**	0.05	**0.26**	**0.43**	**0.09**	**0.30**	**0.22**	**0.30**	**-0.11**	**0.11**	-0.02	**-0.12**	**0.28**
ERA-20C	**0.28**	***-0.07***	***-0.07***	**0.43**	**0.19**	0.02	-0.07	**0.18**	**-0.33**	0.03	**0.11**	**-0.25**	**0.31**
ERA-20CM	**0.24**	-0.04	-0.03	**0.32**	**0.26**	**0.18**	**0.28**	**-0.32**	**0.31**	**0.83**	-0.02	**0.12**	**0.34**
CERA-20C	**0.41**	**0.17**	**0.10**	**0.37**	**0.08**	***0.07***	**0.29**	**0.50**	**-0.58**	**-0.07**	-0.01	**-0.22**	**0.23**
NOAA 20CRv2c	**0.39**	**0.15**	**-0.22**	**0.25**	**0.14**	**0.15**	**0.08**	***-0.07***	**-0.11**	**0.55**	**-0.25**	***-0.05***	**0.50**
NOAA 20CRv2	**0.38**	**0.15**	**-0.21**	**0.18**	**0.14**	**0.23**	**0.19**	-0.02	**-0.20**	**0.56**	**-0.18**	**0.11**	**0.47**
CFSR	**0.33**	**0.12**	**0.10**	**0.19**	**0.37**	**0.21**	**0.19**	**0.11**	**-0.26**	**0.07**	**0.31**	**-0.08**	**0.15**
Obs-raw								***-0.07***	**0.27**	**0.50**			
Obs-homo								**-0.09**	**0.35**	**0.32**			

Atmos. Chem. Phys. Discuss., https://doi.org/10.5194/acp-2017-966
Manuscript under review for journal Atmos. Chem. Phys.
Discussion started: 22 December 2017

Figure Captions:

Figure 1. The multiyear-averaged differences in surface air temperature (T_a, unit: ℃) during the period 1979-2010 from the twelve reanalysis products relative to the homogeneous observations over China, i.e., (**a**) ERA-Interim, (**b**) NCEP-R1, (**c**) MERRA, (**d**) JRA-55, (**e**) NCEP-R2, (**f**) MERRA2, (**g**) ERA-20C, (**h**) ERA-20CM, (**i**) CERA-20C, (**j**) NOAA 20CRv2c, (**k**) NOAA 20CRv2 and (**l**) CFSR. The mainland of China is divided into seven regions: ① Tibetan Plateau, ② Northwest China, ③ Loess Plateau, ④ Middle China, ⑤ Northeast China, ⑥ North China Plain and ⑦ South China.

Figure 2. The impact of inconsistency between station and model elevations on the simulated multiyear-averaged differences in surface air temperature (T_a, unit: ℃) during the study period 1979-2010 over China. The elevation difference (ΔHeight) between station and model consists of the filtering error in spectral model elevation (Δf) and difference in site-to-grid elevation (Δs) due to complex orography. The Δf is derived from the model elevation minus the 'true' elevation at the same model grid from GTOPO30. The GTOPO30 orography is widely used in the reanalyses, e.g., by ECMWF. The colorbar denotes the station elevation (unit: m). The relationship of the T_a difference is regressed on ΔHeight (in the bottom of each subfigure) or Δf and Δs (in the top of each subfigure) with corresponding explained variance.

Figure 3. Taylor diagrams for annual time series of the observed and reanalyzed surface air temperature anomalies (T_a, unit: ℃) from 1979 to 2010 in **(a)** China and **(b-h)** seven subregions. The correlation coefficient, standard deviation and

Atmos. Chem. Phys. Discuss., https://doi.org/10.5194/acp-2017-966
Manuscript under review for journal Atmos. Chem. Phys.
Discussion started: 22 December 2017

Atmospheric Chemistry and Physics Discussions
Open Access
EGU

root-mean-square error (RMSE) were calculated against the observed homogeneous T_a anomaly.

Figure 4. Composite map of partial correlation coefficients of the detrended surface air temperature (T_a, unit: ℃) against surface incident solar radiation (R_s), the precipitation frequency (PF) and surface downward longwave radiation (L_d) during the period 1979-2010 from observations and the twelve reanalysis products. The marker '+' denotes negative partial correlations of T_a with R_s over the Tibetan Plateau for NCEP-R2, ERA-20C and ERA-20CM.

Figure 5. (**a**, **b**) The observed trend in surface air temperature (T_a, unit: ℃/decade) and the simulated trend biases in T_a, (unit: ℃/decade) during the period 1979-2010 from (**c**) raw observations and **(d-o)** the twelve reanalysis products over China with respect to the homogenous observations. The probability distribution functions of all trend biases are shown as colored histogram, and the black stairs are integrated from the trend biases with a significance level of 0.05 (based on two-tailed Student's *t*-test). The cyan/green stairs in (k-n) are estimated the trend biases outside the ensemble ranges whose locations is denotes in the black dots in (k-n).

Figure 6. Composite map of contribution (unit: ℃/decade) of trend biases in three relevant parameters [surface incident solar radiation (R_s, in red), surface downward longwave radiation (L_d, in green) and the precipitation frequency (in blue)] to trend biases in surface air temperature (T_a) during the study period 1979-2010 from the twelve reanalysis products over China.

Figure 7. Contribution (unit: ℃/decade) of trend biases in surface air temperature (T_a)

Atmos. Chem. Phys. Discuss., https://doi.org/10.5194/acp-2017-966
Manuscript under review for journal Atmos. Chem. Phys.
Discussion started: 22 December 2017

Atmospheric Chemistry and Physics Discussions
Open Access

from three relevant parameters, i.e., surface incident solar radiation (R_s, in brown), surface downward longwave radiation (L_d, in light blue) and the precipitation frequency (PF, in deep blue) during the study period 1979-2010 from the twelve reanalysis products over China and seven subregions.

Figure 8. Spatial associations of the simulated trend biases in surface air temperature (T_a) versus relevant parameters among the twelve reanalysis products. The trend calculation was performed during the period 1979-2010 at $1^{\circ}\times1^{\circ}$ grids over China. The probability density functions (unit: %) of these trend biases were estimated from approximately 700 $1^{\circ}\times1^{\circ}$ grids over China. The median values (colored dots) of trend biases in T_a (unit: ℃/decade) were regressed onto those of (**a**) the surface incident solar radiation (R_s, unit: W m^{-2}/decade), (**b**) precipitation frequency (unit: days/decade) and (**c**) the surface downward longwave radiation (L_d, unit: W m^{-2}/decade), using ordinary least squares method (OLS, denoted by dash grey lines) and weighted total least squares method (WTLS, denoted by solid black lines). The regress correlations and slopes were shown as grey and black fonts, respectively. The WTLS were widely applied to the case that has errors on both dependent and independent variables, here such errors as spatial standard deviations of these trend biases (colored error-bars). The 5-95% confidence intervals of regress slopes by the use of WTLS were shown as shading.

Atmos. Chem. Phys. Discuss., https://doi.org/10.5194/acp-2017-966
Manuscript under review for journal Atmos. Chem. Phys.
Discussion started: 22 December 2017

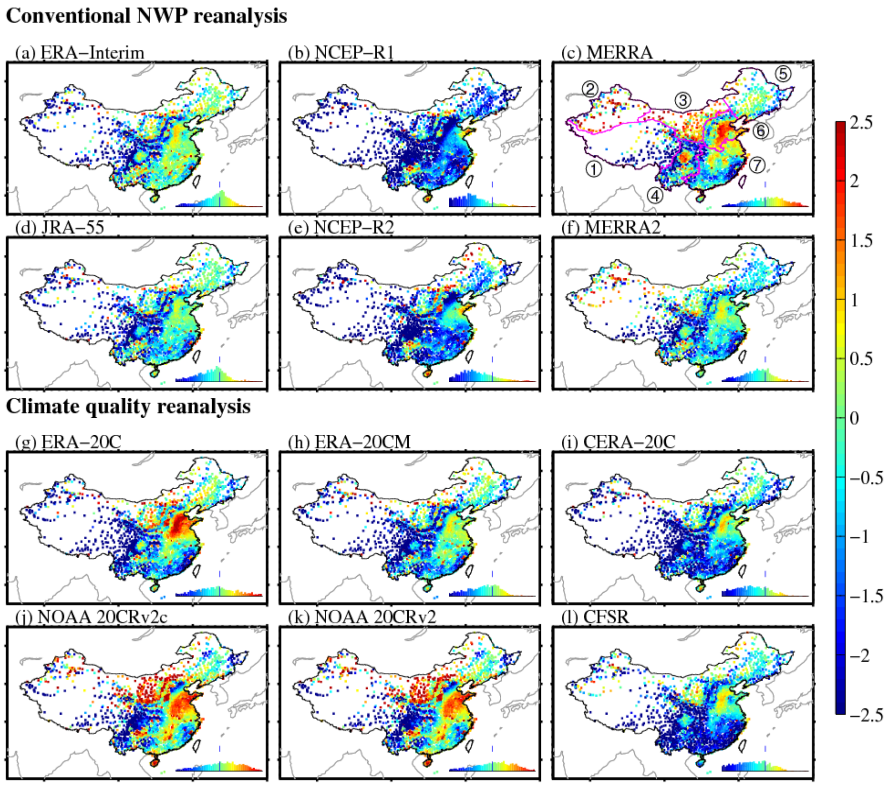

Figure 1. The multiyear-averaged differences in surface air temperature (T_a, unit: ℃) during the period 1979-2010 from the twelve reanalysis products relative to the homogeneous observations over China, i.e., (**a**) ERA-Interim, (**b**) NCEP-R1, (**c**) MERRA, (**d**) JRA-55, (**e**) NCEP-R2, (**f**) MERRA2, (**g**) ERA-20C, (**h**) ERA-20CM, (**i**) CERA-20C, (**j**) NOAA 20CRv2c, (**k**) NOAA 20CRv2 and (**l**) CFSR. The mainland of China is divided into seven regions: ① Tibetan Plateau, ② Northwest China, ③ Loess Plateau, ④ Middle China, ⑤ Northeast China, ⑥ North China Plain and ⑦ South China.

Atmos. Chem. Phys. Discuss., https://doi.org/10.5194/acp-2017-966
Manuscript under review for journal Atmos. Chem. Phys.
Discussion started: 22 December 2017

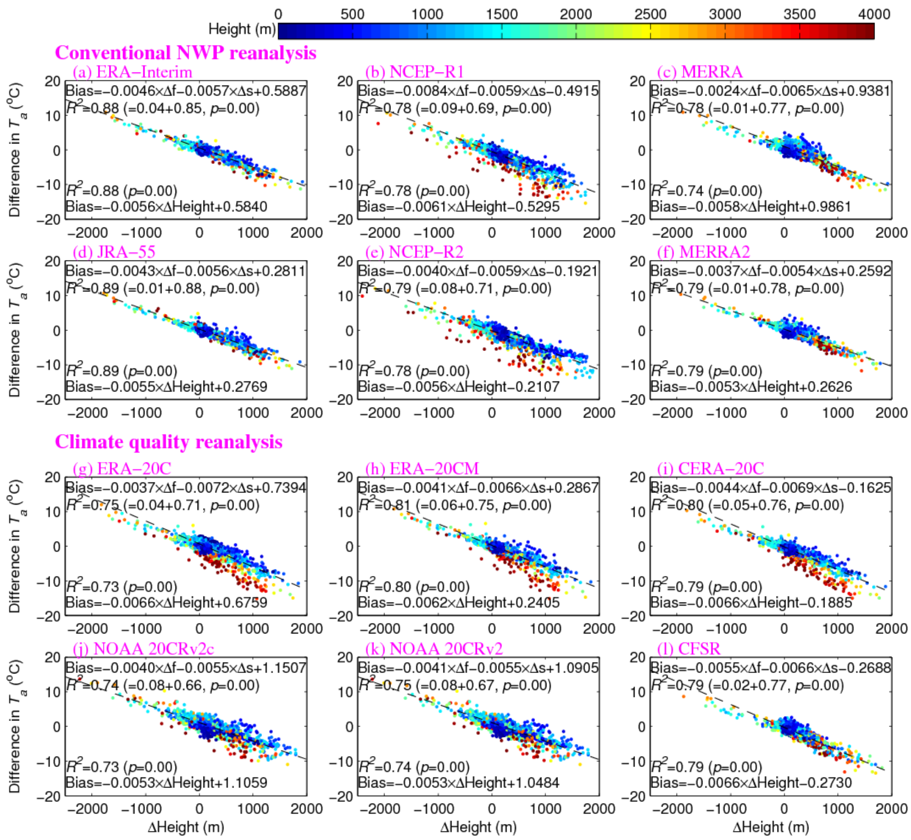

Figure 2. The impact of inconsistency between station and model elevations on the simulated multiyear-averaged differences in surface air temperature (T_a, unit: ℃) during the study period 1979-2010 over China. The elevation difference (ΔHeight) between station and model consists of the filtering error in spectral model elevation (Δf) and difference in site-to-grid elevation (Δs) due to complex orography. The Δf is derived from the model elevation minus the ‘true’ elevation at the same model grid from GTOPO30. The GTOPO30 orography is widely used in the reanalyses, e.g., by ECMWF. The colorbar denotes the station elevation (unit: m). The relationship of the T_a difference is regressed on ΔHeight (in the bottom of each subfigure) or Δf and Δs

Atmos. Chem. Phys. Discuss., https://doi.org/10.5194/acp-2017-966
Manuscript under review for journal Atmos. Chem. Phys.
Discussion started: 22 December 2017

Atmospheric Chemistry and Physics Discussions
Open Access

(in the top of each subfigure) with corresponding explained variance.

Atmos. Chem. Phys. Discuss., https://doi.org/10.5194/acp-2017-966
Manuscript under review for journal Atmos. Chem. Phys.
Discussion started: 22 December 2017

Atmospheric Chemistry and Physics
Discussions

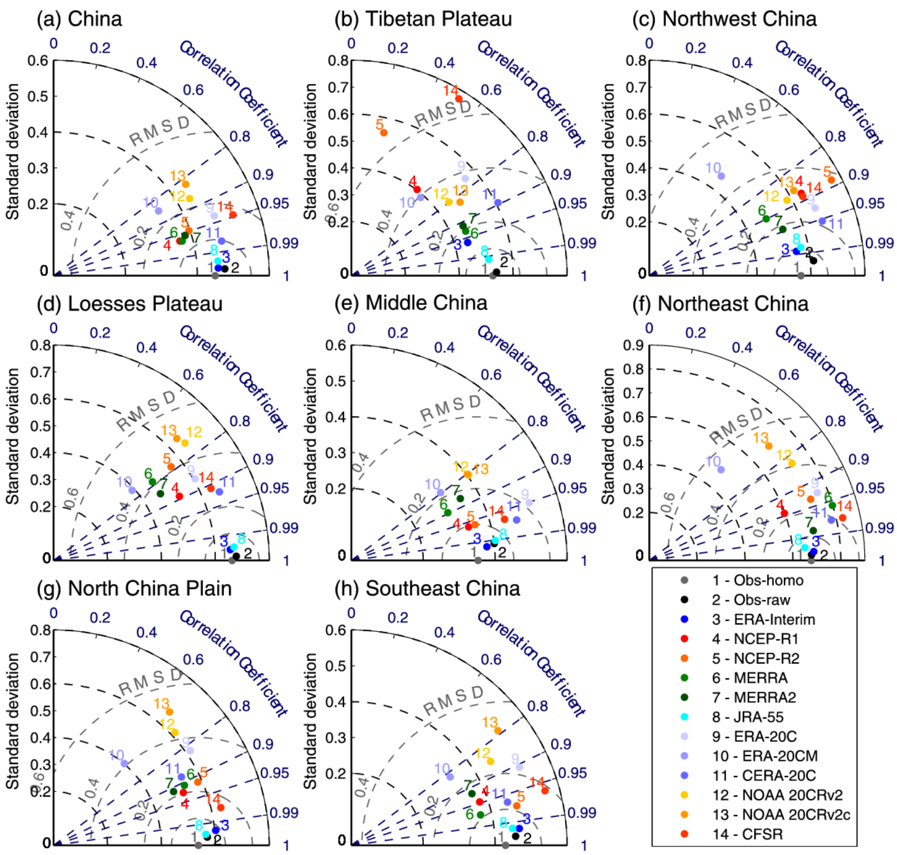

Figure 3. Taylor diagrams for annual time series of the observed and reanalyzed surface air temperature anomalies (T_a, unit: ℃) from 1979 to 2010 in **(a)** China and **(b-h)** seven subregions. The correlation coefficient, standard deviation and root-mean-square error (RMSE) were calculated against the observed homogeneous T_a anomaly.

Atmos. Chem. Phys. Discuss., https://doi.org/10.5194/acp-2017-966
Manuscript under review for journal Atmos. Chem. Phys.
Discussion started: 22 December 2017

Atmospheric Chemistry and Physics
Open Access
Discussions

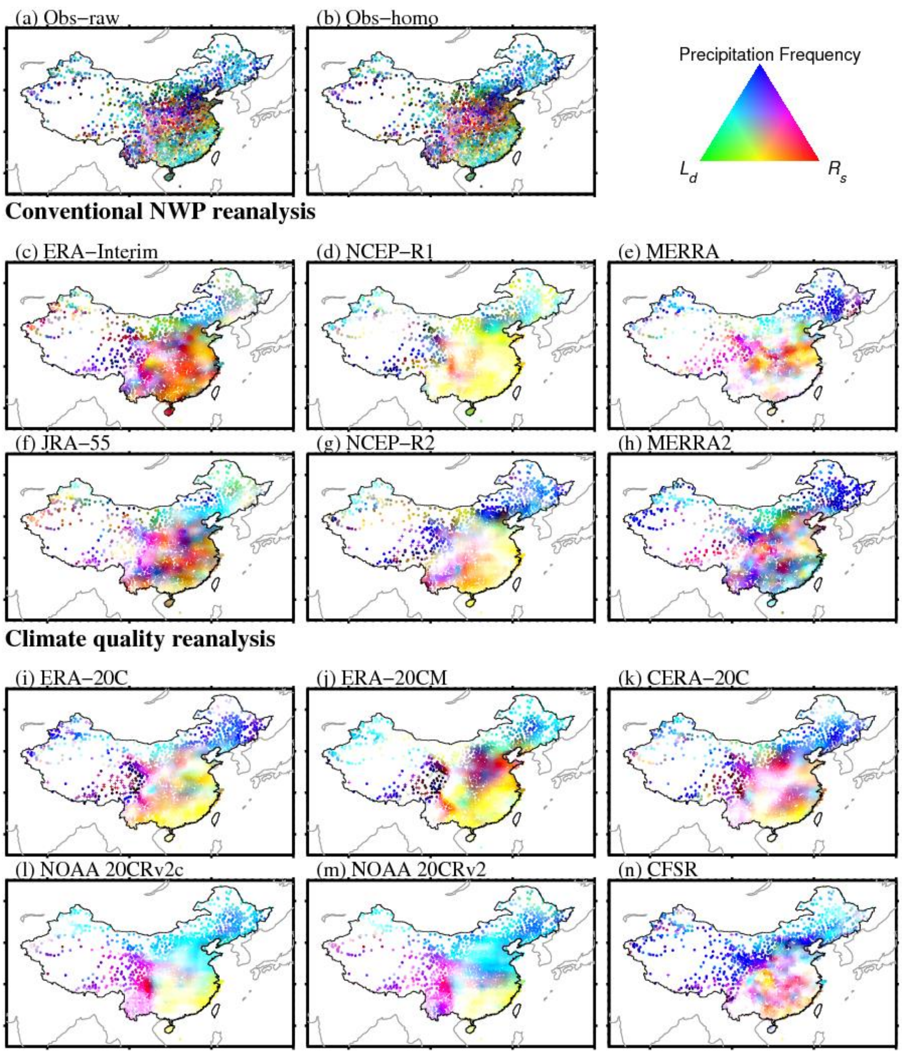

Figure 4. Composite map of partial correlation coefficients of the detrended surface air temperature (T_a, unit: ℃) against surface incident solar radiation (R_s), the precipitation frequency (PF) and surface downward longwave radiation (L_d) during the period 1979-2010 from observations and the twelve reanalysis products. The marker '+' denotes negative partial correlations of T_a with R_s over the Tibetan Plateau for NCEP-R2, ERA-20C and ERA-20CM.

Atmos. Chem. Phys. Discuss., https://doi.org/10.5194/acp-2017-966
Manuscript under review for journal Atmos. Chem. Phys.
Discussion started: 22 December 2017

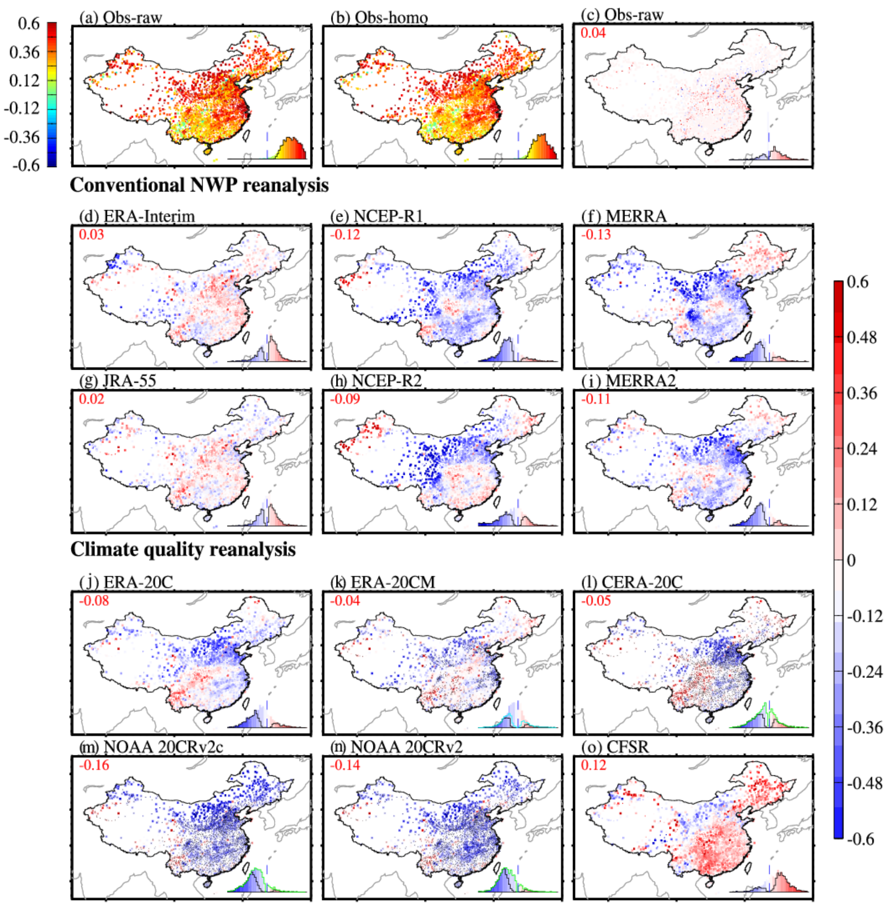

Figure 5. (**a**, **b**) The observed trend in surface air temperature (T_a, unit: ℃/decade) and the simulated trend biases in T_a, (unit: ℃/decade) during the period 1979-2010 from (**c**) raw observations and **(d-o)** the twelve reanalysis products over China with respect to the homogenous observations. The probability distribution functions of all trend biases are shown as colored histogram, and the black stairs are integrated from the trend biases with a significance level of 0.05 (based on two-tailed Student's *t*-test). The cyan/green stairs in (k-n) are estimated the trend biases outside the ensemble ranges whose locations is denotes in the black dots in (k-n).

Atmos. Chem. Phys. Discuss., https://doi.org/10.5194/acp-2017-966
Manuscript under review for journal Atmos. Chem. Phys.
Discussion started: 22 December 2017

Atmospheric Chemistry and Physics
Open Access
Discussions

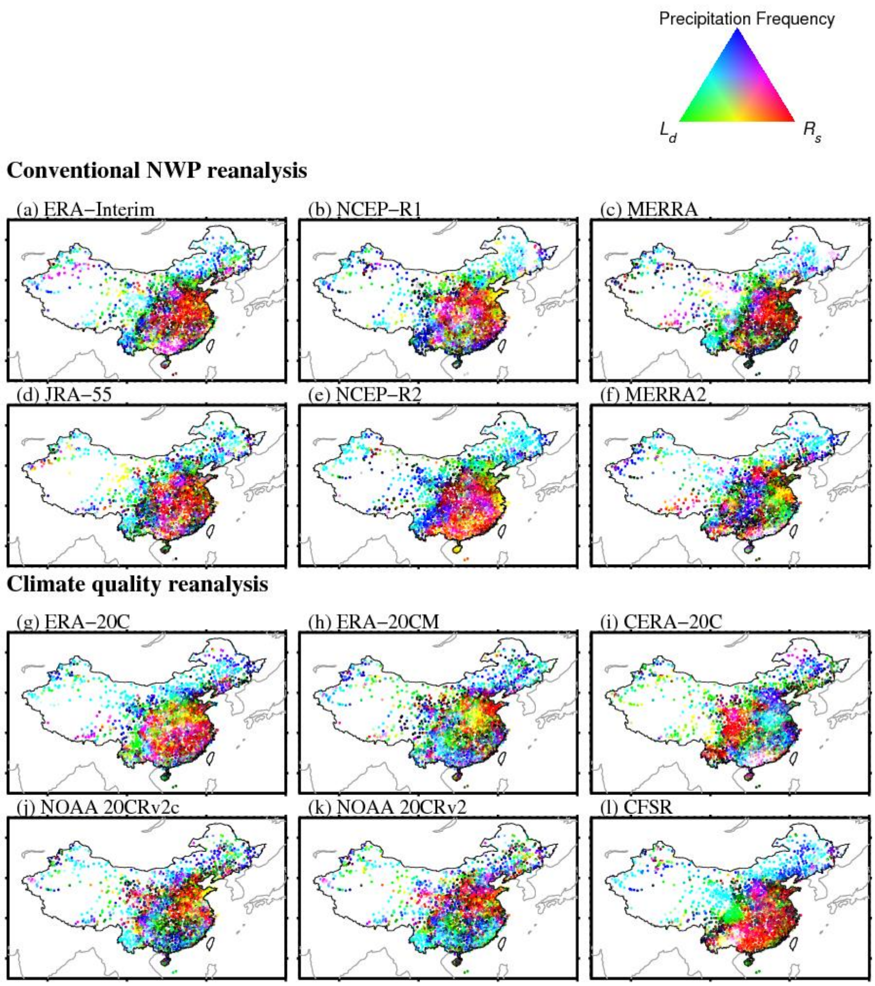

Figure 6. Composite map of contribution (unit: ℃/decade) of trend biases in three relevant parameters [surface incident solar radiation (R_s, in red), surface downward longwave radiation (L_d, in green) and the precipitation frequency (in blue)] to trend biases in surface air temperature (T_a) during the study period 1979-2010 from the twelve reanalysis products over China.

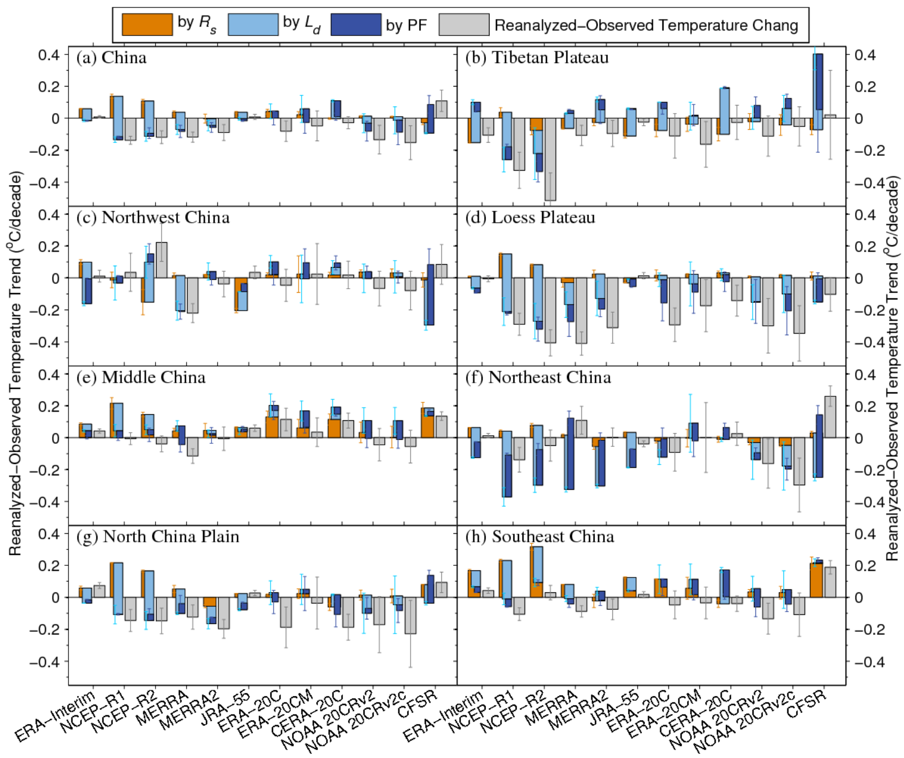

Figure 7. Contribution (unit: ℃/decade) of trend biases in surface air temperature (T_a) from three relevant parameters, i.e., surface incident solar radiation (R_s, in brown), surface downward longwave radiation (L_d, in light blue) and the precipitation frequency (PF, in deep blue) during the study period 1979-2010 from the twelve reanalysis products over China and seven subregions.

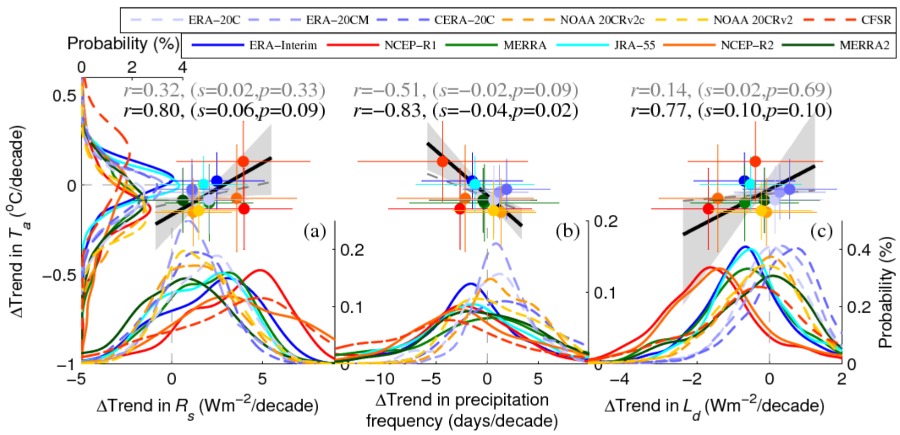

Figure 8. Spatial associations of the simulated trend biases in surface air temperature (T_a) versus relevant parameters among the twelve reanalysis products. The trend calculation was performed during the period 1979-2010 at 1°×1° grids over China. The probability density functions (unit: %) of these trend biases were estimated from approximately 700 1°×1° grids over China. The median values (colored dots) of trend biases in T_a (unit: ℃/decade) were regressed onto those of (**a**) the surface incident solar radiation (R_s, unit: W m^{-2}/decade), (**b**) precipitation frequency (unit: days/decade) and (**c**) the surface downward longwave radiation (L_d, unit: W m^{-2}/decade), using ordinary least squares method (OLS, denoted by dash grey lines) and weighted total least squares method (WTLS, denoted by solid black lines). The regress correlations and slopes were shown as grey and black fonts, respectively. The WTLS were widely applied to the case that has errors on both dependent and independent variables, here such errors as spatial standard deviations of these trend biases (colored error-bars). The 5-95% confidence intervals of regress slopes by the use of WTLS were shown as shading.